An Efficient Assessment of Vulnerability of a Ship to Parametric Roll in Irregular Seas using First Passage Statistics

Abhilash Somayajula[a,b,*], Jeffrey Falzarano[b], Loren Lutes[b]

[a] *Indian Institute of Technology Madras, Chennai, Tamil Nadu, India - 600036*
[b] *Texas A&M University, College Station, TX - 77843*

Abstract

Unlike the traditional displacement vessels, the modern roll-on roll-off (Ro-Ro), container and cruise vessels designed over the past two decades are seen to be prone to dynamic instabilities, which in some cases may lead to capsizing. Although the vulnerability of a design to dynamic instabilities can be assessed through simulations, this approach is time consuming and unsuitable for analyzing several interim designs during the design spiral iterations. Recent global efforts by the International Maritime Organization (IMO) towards a second generation level 2 criterion attempt to adopt a first principles approach without resorting to time consuming numerical simulations or expensive physical model tests. This work provides such a tool for one of the identified capsizing mechanisms known as parametric rolling in a realistic random seaway. The technique of stochastic averaging is applied to a previously developed realistic model for parametric excitation in random waves. A semi-analytic design criterion for the comparative assessment of different hull forms to parametric roll in random seas is formulated in terms first passage statistics of the system. A sensitivity analysis is performed on the C11 container ship hull form to quantify and gain a deeper understanding of the relative importance of both physical parameters (restoring arm and damping) and environmental parameters (wave spectra intensity and characteristic frequency) on the instability.

Keywords: Parametric roll, Stochastic averaging, Volterra GZ method, Irregular Seas, Mean first passage time, Monte Carlo simulation, Dynamic stability, Capsize, Vulnerability
2010 MSC: 00-01, 99-00

1. Introduction

In the past, ship design was regarded as an art acquired through experience and was passed down from generation to generation by ship designers. Over the years, this experience has been codified in terms of prescriptive stability rules that are still widely used today. However, the need for faster ships carrying the same or even larger amounts of cargo has resulted in the evolution of newer advanced hull forms. One such example is the design of a fine form modern container ship characterized by a large bow flare and a broad transom stern to maintain a fine underwater geometry for higher speed and at the same time have enough deck space for carrying more containers. While the prescriptive rules have been sufficient to assess the stability of traditional displacement hull forms, they are inadequate to assess stability of these new modern hull forms.

Within the past two decades, there have been several reports of modern ship types such as Ro-Ro, container and cruise vessels experiencing large amplitude roll motions at sea [1, 2]. These incidents highlight

*Corresponding author
Email addresses: `abhilash@iitm.ac.in; sabhilash89@gmail.com` (Abhilash Somayajula), `jfalzarano@civil.tamu.edu` (Jeffrey Falzarano), `l-lutes@tamu.edu` (Loren Lutes)
URL: `http://www.doe.iitm.ac.in/abhilash/` (Abhilash Somayajula), `http://people.tamu.edu/~jfalzarano/` (Jeffrey Falzarano)

the importance of dynamic stability, which has long been neglected under the prescriptive static stability rules and guidelines required to be followed by ship designers. Due to the increased concern of dynamic stability of vessels at sea, the International Maritime Organization (IMO) has recently decided to re-evaluate the intact stability code to make way for the second generation of intact stability rules focusing on dynamic instabilities such as dead ship rolling, parametric rolling, surf-riding and broaching [3].

The idea behind the second generation of intact stability criterion is to help designers quickly estimate the vulnerability of designs to dynamic instabilities. This criterion should be simple to apply and be able to yield results in a relatively short time frame so that several interim design iterations can be investigated effectively until a satisfactory one is obtained. Since simulations are significantly time consuming and time is a big factor while evaluating interim designs, analytical methods are appropriate for this problem. Although analytical methods are limited by simplifying assumptions, they provide an almost instantaneous result and allow the designer to rank various designs according to their vulnerability to the concerned dynamic instability. In this paper a previously developed analytical model [4, 5] for parametric roll is analyzed using the technique of stochastic averaging to come up with a semi-analytic criterion to assess the stability of any vessel to parametric roll in irregular seas.

The paper is organized into nine sections including the introduction. A brief overview of literature reporting various methods used to analyze probabilistic response of a nonlinear systems excited by a random input is provided in section 2. It also discusses the advantages of the stochastic averaging method over other techniques. Section 3 describes the energy-phase formulation for the roll motion of a vessel using a previously developed modeling technique - Volterra $\overline{GZ}$ method [5]. Section 4 describes the principles of stochastic averaging from a practical perspective and discusses the physical meaning of the assumptions involved. Section 5 discusses the solution of the Fokker-Plank-Kolmogorov equation when stationarity is assumed. Section 6 discusses the solution of the first passage problem for parametrically excited roll motion. The results from stochastic averaging are compared with Monte Carlo simulations and reported in section 7. The conclusions of the study are reported in section 8.

2. Literature Review

Since a vessel at sea is always experiencing a random wave environment, it is important to consider dynamic stability in a random sea state instead of regular waves. It is well known that for a linear system excited by a Gaussian excitation, the response also follows a Gaussian distribution. However, when the equations of motion are nonlinear, such as for the problem of parametric roll, the probability distribution of the response can deviate significantly from Gaussian distribution [6]. Obtaining a probabilistic description of the response for such nonlinear systems is often a challenge. Some of the analytical methods available to analyze the problem of nonlinear random vibration include Markov methods [7], equivalent linearization [8], equivalent non-linearization [9, 10], moment and cumulant closure techniques [11, 12, 13], perturbation methods [14], stochastic averaging [15] and numerical simulations.

Markov methods involve solving for the probability distribution of response by numerically solving the corresponding Fokker-Planck-Kolmogorov (FPK) equation, also known as Kolmogorov's forward equation [16]. Markov methods are typically restricted to systems that are excited by a pure white noise. However, it can be extended to systems excited by colored (non-white) noise by introducing a filter to transform white noise to the colored noise [13, 17]. After introducing the filter, Markov method can then be applied to the extended system that is a combination of the original system and the transform filter. Su and Falzarano (2011) [13] showed that for a ship system excited by an irregular beam sea, a fourth order filter is needed to accurately model the narrow-banded wave excitation using a white noise input. Expressing systems excited by colored excitation as systems excited by white noise comes at the cost of introducing more state variables (corresponding to the filter), which increases the complexity of the problem. This disadvantage is sometimes referred to as the curse of dimensionality [13].

If the initial probability distribution of the system is chosen appropriately such that the system is stable and eventually achieves stationarity, the time derivative in the FPK equation can be set to zero and the corresponding equation can be solved to obtain a stationary probability distribution of the response.

However, exact analytical expressions exist only for very few special cases (see for example Caughey [18]). For higher order systems (with many state variables) very few exact solutions are available.

In cases where exact solutions are unavailable, many researchers have investigated the numerical approach to solve the FPK equation. Some of the methods in this approach include iterative methods [19], series expansion methods [11, 12], random walk analogies and path integral methods [20, 21, 7]. Probability density evolution methods [22], discretized Chapman-Kolmogorov equation numerical schemes (also known as numerical path integration) [23, 24], as well as Wiener path integral (i.e. functional integral) based solution techniques [25, 26] have received significant attention in recent years to solve the FPK equation with lesser computational efforts. However, obtaining exact solutions to the FPK equation is still time consuming and is impractical for assessing several design iterations in a short time.

The method of moments is an alternative to the FPK equation where algebraic equations governing the various moments of the response are constructed directly using the differential equation governing the response [16]. For nonlinear systems, deriving expressions for higher moments often results in cross moments between the excitation and response and higher order response moments. In order to simplify the cross moments between the excitation and response, a simplifying approximation of delta correlated excitation (e.g. white noise) is made. To uniquely solve for the moments of the system, the higher order response moments are expressed in terms of the lower order moments using specific closure techniques. One of the common closure techniques is the Gaussian closure technique that involves expressing the higher order moments in terms of just the first two moments. An application of this technique to ship roll motion in beam seas was investigated by Francescutto and Naito (2004) [27]. However, there are other closure techniques that allow a better capture of the stochastic nature of the response of a strongly nonlinear system. Higher order non-Gaussian cumulant neglect closures were investigated by Su and Falzarano (2011) [28, 13] and found to better capture the response characteristics than the Gaussian closure method for the problem of ship roll in beam seas.

So far all the methods described above try to approximate the response as a diffusion process (a Markov process with almost surely continuous sample paths) by imposing a restriction that the excitation process is pure white noise. The downside of this restriction is that the number of state variables increases, making the problem harder. However, the technique of stochastic averaging originally introduced by Stratonovich (1963,1967) [11, 12] allows approximating the response as a diffusion process while keeping the number of state variables the same or even less than that in the original system. Also the stochastic averaging technique could be applied to systems excited by colored noise without needing to introduce a filter to model the conversion from white to colored noise. For this reason, in the recent years, the stochastic averaging technique has received much attention.

Although, this approach is only applicable to a specific class of problems where the bandwidth of the excitation is larger than that of the response, it has found numerous applications in several branches of engineering including radio engineering, structural engineering and ocean engineering. Since its proposition by Stratonovich [11], this technique has been examined in detail by many researchers to provide mathematical rigor to the approach [29, 30] and is now formalized as the well known Stratonovich-Khas'minskii theorem. According to Roberts (1989) [31], and Lin and Cai (2004) [32] the approach can be regarded as the generalization of the deterministic averaging due to Bogoliubov and Mitropolsky (1961) [33] extended to systems with random excitation.

Although stochastic averaging has been extensively used to study the response of structures to random excitation [32, 34], Roberts (1982) [15] was one of the first to apply it to the ship roll problem in beam seas. Some of the recent works in this area include Chai et al. (2018) [35] and Su and Falzarano (2012, 2013) [36, 37], where the focus was on ship rolling in beam seas. Roberts (1982) [38] also investigated the parametric roll response in irregular longitudinal seas. However, this work was based on a very simplified model and assumed weak nonlinearity, and it has been fairly well established [39, 3, 40, 4] that parametric rolling is a strongly nonlinear phenomenon characterized by higher order time varying stiffness terms. Dostal et al. (2012, 2014) [41, 42] have investigated the application of stochastic averaging to the problem of parametric excitation using the Grim's effective wave approach and modeling the roll restoring arm as a cubic polynomial. However, for a wave with its crest near the midship of the vessel the roll restoring arm exhibits an initial hardening and eventual softening, which requires at least a 5^{th} or higher degree polynomial

Table 1: Details of the C11 hull form

Particulars	**Value**
Length between perpendiculars L_{pp} (m)	262.00
Breadth B (m)	40.00
Depth D (m)	24.45
Mean Draft T (m)	12.32
Displacement $\Delta = \rho\nabla$ (tonnes)	76056.00
Vertical Center of Gravity $\overline{KG}$ (m)	18.32
Metacentric Height $\overline{GM}$ (m)	1.973
Roll Natural Period T_n (sec)	22.78
Forward Speed of the Vessel U (knots)	8.00

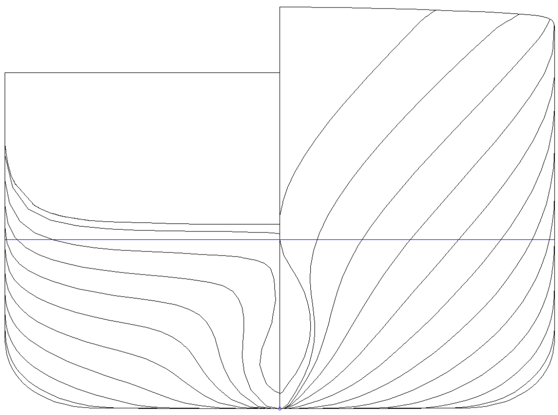

Figure 1: Body plan of the C11 hull form

to capture this effect [43]. Somayajula and Falzarano (2018) [5] show that a 11^{th} degree polynomial is needed to accurately capture the roll restoring arm in waves for the C11 hull form.

Over the years there have been several models proposed for parametric roll taking into account increasing levels of complexity - coupled higher order Taylor series model [44], Grim's effective approach [45, 46], Volterra GM model [47, 48, 49, 50] and Volterra GZ model [51, 5]. In this paper, the stochastic averaging technique is applied to a previously developed model [4, 5] for parametric roll. The analysis further demonstrates the ability of the method to assess stability of a vessel under parametric excitation without the need to simulate long time histories.

All the results reported in this paper are generated for the standard C11 hull form, which is slightly modified from the hull form of APL China. This hull form is particularly chosen since it is known to be vulnerable to parametric roll phenomenon [1]. The particulars of the vessel are listed in Table 1. Figure 1 shows the contours of the hull sections at equally spaced longitudinal positions and is known as the body plan. The left half of the body plan shows the sections to the aft of midship and the right half shows the sections forward of midship. The blue line denotes the calm waterline of the vessel.

3. Energy-Phase Formulation

The dimensional roll equation of motion of a vessel which has a port-starboard symmetry and is experiencing head on waves is given by (1)

$$\begin{aligned}[I_{44} + A_{44}(\infty)]\ddot{\phi} + \int_{-\infty}^{u} K_{44}(u-v)\dot{\phi}(v)dv \\ + B_1\dot{\phi} + B_2\dot{\phi}|\dot{\phi}| + \rho g \nabla_0 \overline{GZ}(u,\phi) = 0 \end{aligned} \tag{1}$$

where

ϕ denotes the roll angle that is a function of dimensional time u

I_{44} is the mass moment of inertia

$A_{44}(\infty)$ is the infinite frequency added mass moment of inertia

$K_{44}(\tau)$ is the impulse response function for the roll mode of motion

B_1 and B_2 are the linear and quadratic viscous roll damping coefficients

∇_0 is the calm water displacement of the vessel

$\overline{GZ}(u,\phi)$ is the effective time varying nonlinear roll restoring arm in irregular waves which also includes the effect of time varying displacement (refer to Somayajula and Falzarano [5] for more details)

ρ is the density of sea water and has a value of 1025 kg/m^3

g is the acceleration due to gravity and has a value of 9.81 m/s^2

Since potential damping at the roll natural frequency is small, the viscous effects play a significant role and estimation is needed. Typically they are estimated using model scale free decay experiments or forced roll experiments. However, these may not necessarily reflect the actual viscous damping in the presence of waves. If experimental time histories of motion of a vessel are available, then these damping coefficients can be estimated through system identification [52, 53, 54]. When model scale experimental data is not available, recourse may be taken to empirical methods. The viscous roll damping in this work is approximated by a linear and a quadratic term that are empirically calculated using the state of the art approach described by Himeno [55, 56]. The details of the empirical method implemented and its validation with experimental data can be found in works of Falzarano et al. (2015) [57].

The linear undamped natural frequency of the vessel is given by

$$\omega_n = \sqrt{\frac{\rho g \nabla_0 \overline{GM}_0}{[I_{44} + A_{44}(\omega_n)]}} \tag{2}$$

where $A_{44}(\omega_n)$ denotes the added mass moment of inertia at the undamped linear roll natural frequency ω_n and $\overline{GM}_0$ is known as the calm water metacentric height of the vessel which denotes the vertical distance between the center of gravity of the vessel and its metacenter. When a vessel rolls, the position of the center of buoyancy changes (from B_0 to B) due to the change in underwater geometry as shown in Figure 2. The metacenter M is the point where the vertical line through the new center of buoyancy intersects with the vertical line through original center of buoyancy. Figure 2 shows a scenario in waves where W_1L_1 is the new waterline in waves and W_0L_0 is the calm waterline. M_0 represents the limiting position of metacenter M when the vessel roll angle is zero and the vessel is floating in calm water. The metacentric height $\overline{GM}_0$ is a measure of the initial static stability of a vessel. A larger $\overline{GM}_0$ implies greater roll restoring stiffness.

In case of parametrically excited roll motion, it is well known that the response is narrow banded around the linear undamped natural frequency of the vessel ω_n. Thus for the case of a parametrically excited system

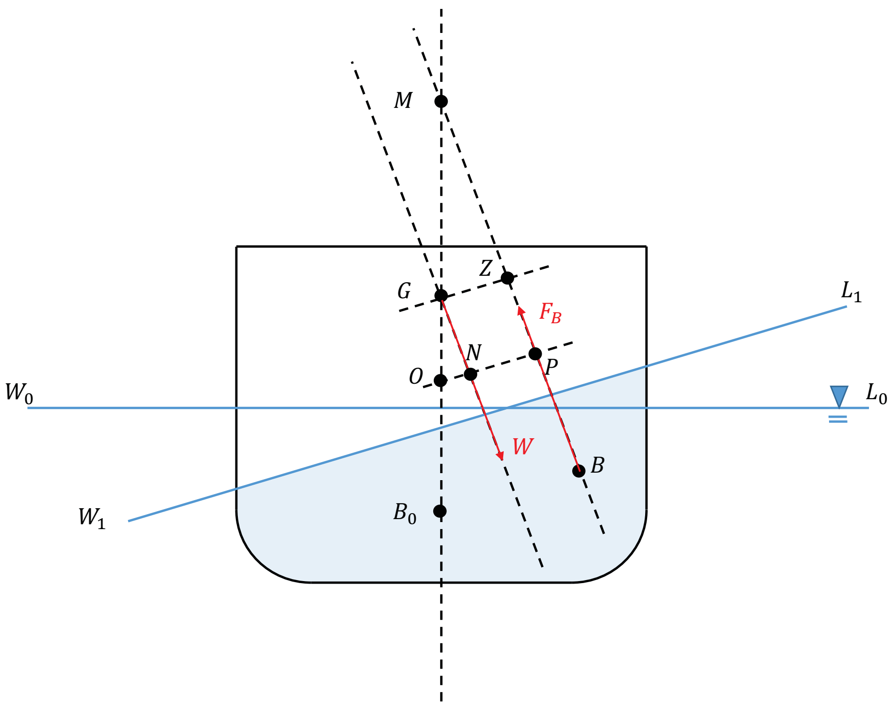

Figure 2: Roll Restoring Moment

it is a reasonable approximation to use the roll added mass moment of inertia and radiation damping at the natural frequency ω_n instead of the convolution integral. Under this assumption, the roll equation of motion is given by

$$[I_{44} + A_{44}(\omega_n)]\ddot{\phi} + B_{44}(\omega_n)\dot{\phi} + B_1\dot{\phi} + B_2\dot{\phi}|\dot{\phi}| + \rho g \nabla_0 \overline{GM}_0 \frac{\overline{GZ}(u,\phi)}{\overline{GM}_0} = 0 \tag{3}$$

where $A_{44}(\omega_n)$ and $B_{44}(\omega_n)$ are the frequency dependent added mass moment of inertia and radiation damping calculated at the roll natural frequency ω_n. The time varying restoring arm $\overline{GZ}(u,\phi)$ can be separated into the calm water component $\overline{GZ}_0(\phi)$ and the time varying component $\Delta\overline{GZ}(u,\phi)$ as shown below.

$$\overline{GZ}(u,\phi) = \overline{GZ}_0(\phi) + \Delta\overline{GZ}(u,\phi) \tag{4}$$

The time varying restoring arm can be expressed as an odd polynomial of roll angle ϕ with time varying coefficients $K_1(u)$, $K_3(u)$, $K_5(u)$, ... as shown below. Each of the $K_i(u)$ $(i = 1,3,5,...)$ can further be separated into two parts - a time independent part $K_i^{(0)}$ $(i = 1,3,5,...)$ corresponding to calm water restoring arm and a time dependent part $K_i^{(1)}(u)$ $(i = 1,3,5,...)$ corresponding to time variation of restoring arm in waves.

$$\overline{GZ}(u,\phi) = K_1(u)\phi + K_3(u)\phi^3 + K_5(u)\phi^5 + ... \tag{5}$$

$$= (K_1^{(0)} + K_1^{(1)}(u))\phi + (K_3^{(0)} + K_3^{(1)}(u))\phi^3 + (K_5^{(0)} + K_5^{(1)}(u))\phi^5 + ... \tag{6}$$

The non-dimensional calm water restoring arm can be expressed as an odd polynomial function of roll angle ϕ:

$$\frac{\overline{GZ}_0(\phi)}{\overline{GM}_0} = \alpha_1\phi + \alpha_3\phi^3 + \alpha_5\phi^5 + ... \tag{7}$$

where $\alpha_1, \alpha_3, \alpha_5, ...$ represent the non-dimensional coefficients of the calm water restoring arm and are given by

$$\alpha_1 = \frac{K_1^{(0)}}{\overline{GM}_0} = 1 \qquad \alpha_3 = \frac{K_3^{(0)}}{\overline{GM}_0} \qquad \alpha_5 = \frac{K_5^{(0)}}{\overline{GM}_0} \qquad ... \tag{8}$$

The non-dimensional time varying component of the restoring arm can be expressed as

$$\frac{\Delta\overline{GZ}(u,\phi)}{\overline{GM}_0} = \varepsilon p_1(t)\phi + \varepsilon p_3(t)\phi^3 + \varepsilon p_5(t)\phi^5 + ... \tag{9}$$

where $\varepsilon p_1(t), \varepsilon p_3(t), \varepsilon p_5(t), ...$ represent the non-dimensional time varying coefficients of the restoring arm and are given by

$$\varepsilon p_1(t) = \frac{K_1^{(1)}(u)}{\overline{GM}_0} \qquad \varepsilon p_3(t) = \frac{K_3^{(1)}(u)}{\overline{GM}_0} \qquad \varepsilon p_5(t) = \frac{K_5^{(1)}(u)}{\overline{GM}_0} \qquad ... \tag{10}$$

and t represents the non-dimensional time given by $t = \omega_n u$. Thus the roll equation shown in (3) can be further simplified and expressed in its non-dimensional form as shown in (11)

$$\begin{aligned} &\ddot{x} + \varepsilon^2\delta_1\dot{x} + \varepsilon^2\delta_2\dot{x}|\dot{x}| + \left[\alpha_1 x + \alpha_3 x^3 + \alpha_5 x^5 + ...\right] \\ &+ \left[\varepsilon p_1(t)x + \varepsilon p_3(t)x^3 + \varepsilon p_5(t)x^5 + ...\right] = 0 \end{aligned} \tag{11}$$

where

$$x = \phi \qquad \dot{(\ )} = \frac{d}{dt}(\ ) = \frac{1}{\omega_n}\frac{d}{du}(\ ) \tag{12}$$

The linear and quadratic damping coefficients b_1 and b_2 are defined as shown in (13) and (14).

$$\varepsilon^2\delta_1 = \frac{B_{44}(\omega_n) + B_1}{[I_{44} + A_{44}(\omega_n)]\omega_n} = b_1 \tag{13}$$

$$\varepsilon^2\delta_2 = \frac{B_2}{[I_{44} + A_{44}(\omega_n)]} = b_2 \tag{14}$$

Note that the small parameter ε is introduced to represent the relative order of various terms in the equation of motion. The scaling ensures that the standard deviation of the response is $O(\varepsilon)$ as $\varepsilon \to 0$ and does not imply that the excitation is weak [58].

It is assumed that the wave elevation in the ocean is a zero mean Gaussian stationary process and is characterized by a Bretschneider wave elevation spectrum. The mathematical expression for the Bretschneider spectrum as a function of significant wave height H_s and peak period T_p is given by (15). Significant wave height H_s is defined as the mean wave height (valley to peak) of the highest third of the waves and peak period T_p is defined as the period corresponding to the peak of the spectrum.

$$S(\omega) = \frac{5T_pH_s^2}{32\pi}\left(\frac{2\pi}{\omega T_p}\right)^5 e^{-\frac{5}{4}\left(\frac{2\pi}{\omega T_p}\right)^4} \tag{15}$$

For a ship moving with forward speed U, the apparent frequency of encounter of waves ω_e as perceived by an observer aboard the ship is different from the actual frequency of the waves ω. The two frequencies can be related to each other by Doppler's theory and this is shown in (16) where β is the wave direction measured anti-clockwise from the positive x-axis. The latter expression is obtained using the deep water dispersion relationship ($\omega^2 = gk$).

$$\omega_e = \omega - kU\cos\beta = \omega - \frac{\omega^2}{g}U\cos\beta \tag{16}$$

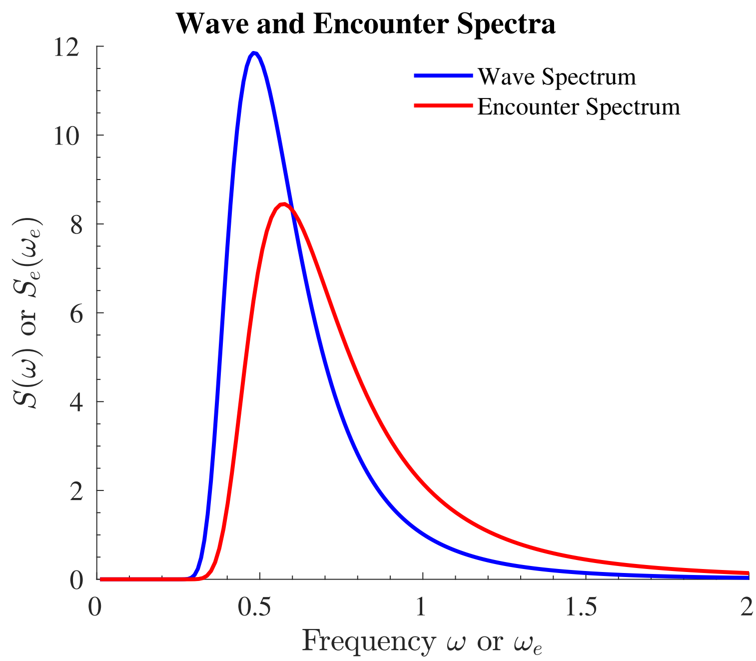

Figure 3: Bretschneider and encounter spectra of wave elevation for $H_s = 8\ m$, $T_p = 13\ s$, $\beta = 180^0$ and $U = 8$ knots

The effect of encounter frequency also changes the observed spectrum of the sea. However, the energy under both the original wave spectrum and the encounter wave spectrum must be the same, which leads to the following expression for the encounter spectrum. Figure 3 shows the plot of the Bretschneider spectrum and its corresponding encounter spectrum for parameters $H_s = 8\ m$, $T_p = 13\ s$, $\beta = 180^0$ and $U = 8$ knots.

$$S_e(\omega_e) = S(\omega)\left|\frac{d\omega}{d\omega_e}\right| = \frac{S(\omega)}{\left|1 - \frac{2U\cos\beta}{g}\omega\right|} \tag{17}$$

For obtaining a wave realization the encounter spectrum $S_e(\omega_e)$ is discretized into $N = \frac{T_{max}}{2du}$ points where T_{max} is the simulation time and du is the discrete time step. The discrete frequency step is given by $\Delta\omega_m = \frac{2\pi}{T_{max}}$. The irregular sea is obtained by linear superposition of N harmonic components as shown below.

$$\eta(u,x) = \frac{1}{2}\sum_{m=1}^{N} a_m\left[e^{i(-k_m(x\cos(\beta)+y\sin(\beta))+\omega_m u+\epsilon_m)} + e^{-i(-k_m(x\cos(\beta)+y\sin(\beta))+\omega_m u+\epsilon_m)}\right] \tag{18}$$

where

$a_m = \sqrt{2S_e(\omega_m)\Delta\omega_m}$ is the amplitude of the m^{th} harmonic component

ω_m and k_m are the encounter frequency and the wave number of the m^{th} harmonic component respectively

ϵ_m is the phase of the m^{th} harmonic component and is realized from a uniform random variable varying in the range $[0\ 2\pi]$

For a head sea condition $\beta = 180^0$ and the wave elevation is given by (19).

$$\eta(u,x) = \frac{1}{2}\sum_{m=1}^{N} a_m\left[e^{i(k_m x+\omega_m u+\epsilon_m)} + e^{-i(k_m x+\omega_m u+\epsilon_m)}\right] \tag{19}$$

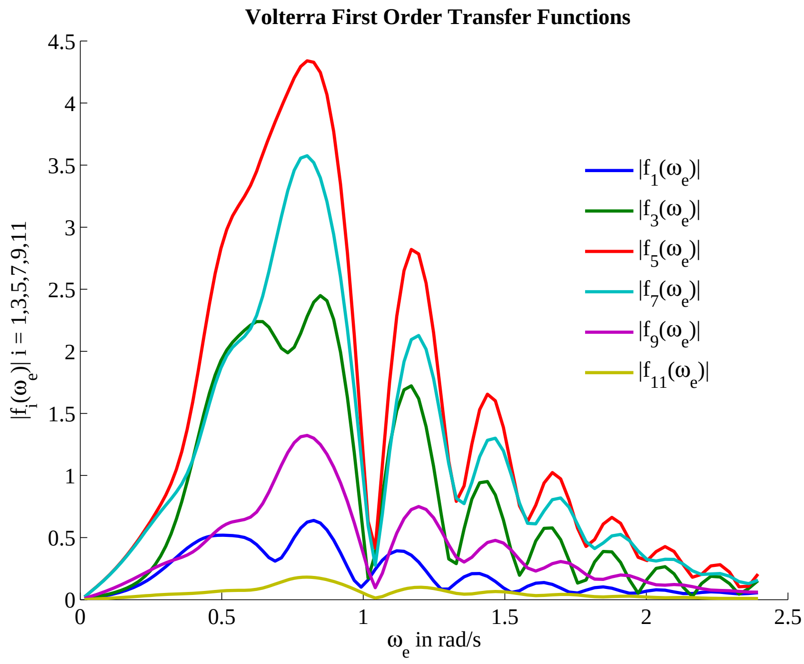

Figure 4: First order transfer functions (TRFs) $f_i(\omega_e)$

The time varying coefficients $K_1^{(1)}(u),\ K_3^{(1)}(u),\ K_5^{(1)}(u),\ \ldots$ in the polynomial expression of $\overline{GZ}$ described in (6) are obtained by first order Volterra transfer functions $f_1(u,)\ f_3(u),\ f_5(u),\ \ldots$ as shown in (20), in which $\bar{f}_i$ denotes the complex conjugate of f_i.

$$K_i^{(1)}(u) = \frac{1}{2}\sum_{m=1}^{N} a_m \left[f_i(\omega_m)e^{i(\omega_m u+\epsilon_m)} + \bar{f}_i(\omega_m)e^{-i(\omega_m u+\epsilon_m)} \right] \text{ for } i = 1, 3, 5, \ldots \tag{20}$$

The frequency dependent Volterra transfer functions (TRFs) $f_1(\omega_e),\ f_3(\omega_e),\ f_5(\omega_e),\ \ldots$ depend on the geometry of the vessel. The ship hull is separated into several transverse sections along the length of the hull and hydrostatic restoring moment at each section is expressed as a Taylor expansion about a mean draft. The contributions of each transverse sections are then integrated along the length to yield Volterra transfer functions for time varying coefficients of the restoring moment of ship in waves. The plots of the transfer functions are shown in Figure 4. For more modeling details of Volterra $\overline{GZ}$ method and the derivation of the first order Volterra transfer functions please refer to Somayajula [4] or Somayajula and Falzarano [5].

A more general form of the non-dimensional roll equation can be written as

$$\ddot{x} + \varepsilon^2 F(\dot{x}) + G(x) + \varepsilon G_1(t,x) = 0 \tag{21}$$

where $F(\dot{x})$ is a nonlinear damping function, $G(x)$ is the time invariant nonlinear restoring moment and $G_1(t,x)$ is the time varying restoring moment in waves. For our specific example $F(\dot{x})$, $G(x)$ and $G_1(t,x)$

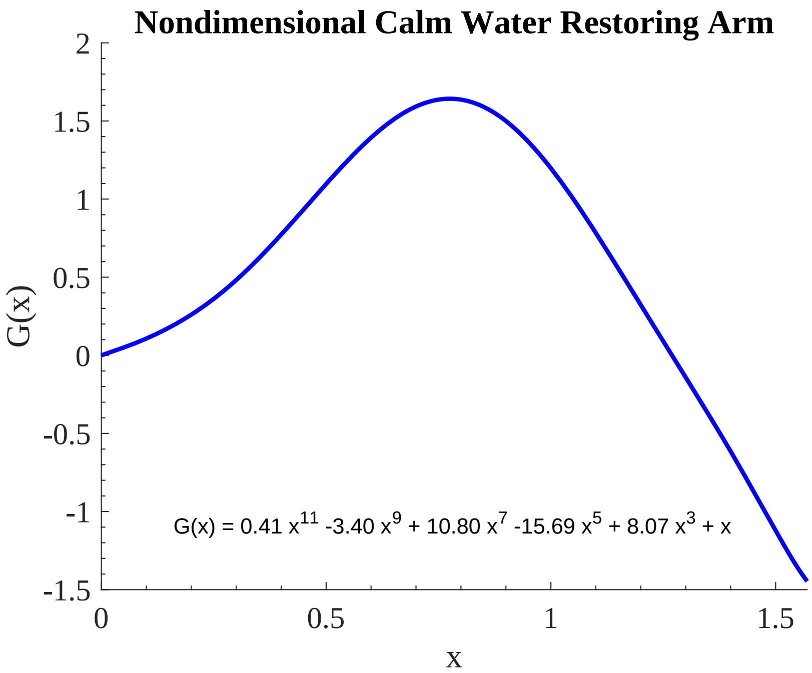

Figure 5: Non-dimensionalized calm water restoring arm

are given by

$$\varepsilon^2 F(\dot{x}) = b_1\dot{x} + b_2\dot{x}|\dot{x}| \tag{22}$$

$$\overline{GZ}(t,x) = \overline{GZ}_0(x) + \varepsilon\overline{GZ}_1(t,x) \tag{23}$$

$$G(x) = \frac{\overline{GZ}_0(x)}{\overline{GM}_0} = \sum_{j=1,3,5,\ldots}^{2n_q-1} \alpha_j x^j \tag{24}$$

$$G_1(t,x) = \frac{\overline{GZ}_1(t,x)}{\overline{GM}_0} = \sum_{j=1,3,5,\ldots}^{2n_q-1} p_j(t) x^j \tag{25}$$

where $p_j(t)$ represents the parametric time varying coefficients of $\overline{GZ}$ curve and are calculated using Volterra $\overline{GZ}$ formulation detailed in Somayajula and Falzarano (2018) [5]. The degree of the restoring arm is given by $2n_q - 1$. Typically, restoring term $G(x)$ is modelled as a cubic polynomial for studying roll motion in beam seas. However, parametric roll is a more complicated phenomenon where the hull geometry plays a significant role on the dynamics. The roll restoring arm exhibits strong nonlinearities, especially when the crest of the incident wave is around the midship of the vessel. The cubic polynomial model cannot capture the effect of initial hardening and eventual softening due to coupling effects of incident wave, instantaneous heave and pitch motions and hull geometry. Mathematically a 5^{th} or higher degree polynomial is required to capture the initial hardening and eventual softening effect. Somayajula and Falzarano (2018) [5] have shown that for the hull form chosen in this study an 11^{th} degree polynomial is needed to effectively capture the variation of restoring arm in waves. In this work too $n_q = 6$ is used to result in a 11^{th} degree polynomial restoring curve. Figure 5 shows the plot of $G(x)$ for the C11 hull form.

The total energy $E(t)$ is defined as the sum of kinetic and potential energy as shown in

$$E = \frac{\dot{x}^2}{2} + U(x) \tag{26}$$

where $U(x)$ is the potential energy associated with the nonlinear restoring moment $G(x)$ and is given by

$$U(x) = \int_0^x G(\xi) d\xi \tag{27}$$

The equation of motion can be recast in terms of energy $E(t)$ and a related phase angle $\theta(t)$ defined such that the following transformations hold and also satisfy (26).

$$\operatorname{sgn}(x)\sqrt{U(x)} = \sqrt{E}\cos(\theta) \tag{28}$$

$$\frac{\dot{x}}{\sqrt{2}} = -\sqrt{E}\sin(\theta) \tag{29}$$

where

$$\operatorname{sgn}(x) = \begin{cases} 1 & \text{if } x \geq 0 \\ -1 & \text{if } x < 0 \end{cases} \tag{30}$$

The differential equation governing $E(t)$ is obtained by differentiating (26) with respect to time and is given by

$$\begin{aligned} \dot{E} &= \ddot{x}\dot{x} + G(x)\dot{x} \\ &= \dot{x}\left[-\varepsilon^2 F(\dot{x}) - \varepsilon G_1(t, x)\right] \\ &= \varepsilon^2 \left(f(E, \theta)\sqrt{2E}\sin(\theta)\right) + \varepsilon \left(g_1(t, E, \theta)\sqrt{2E}\sin(\theta)\right) \end{aligned} \tag{31}$$

where

$$f(E, \theta) = F(\dot{x}) \tag{32}$$

$$g_1(t, E, \theta) = G_1(t, x) \tag{33}$$

Note that the first term in (31) depends on the damping present in the system. This term is always negative and represents the loss of energy. The differential equation governing the phase angle $\theta(t)$ is obtained using (28) and (29) and is given by

$$\begin{aligned} \dot{\theta} &= \frac{d}{dt}\left[\tan^{-1}\left(-\frac{\dot{x}}{\sqrt{2U(x)}}\right)\right] \\ &= \frac{1}{1 + \left(\frac{\dot{x}^2}{2U(x)}\right)} \frac{-1}{\sqrt{2}} \frac{\ddot{x}\sqrt{U(x)} - \frac{\dot{x}^2 G(x)}{2\sqrt{U(x)}}}{U(x)} \\ &= \frac{-\cos^2\theta}{\sqrt{2}}\left[\frac{-\varepsilon^2 f(E, \theta) - \varepsilon g_1(t, E, \theta) - g(E, \theta)}{\sqrt{E}\cos(\theta)} - \frac{\tan^2(\theta) g(E, \theta)}{\sqrt{E}\cos(\theta)}\right] \\ &= \varepsilon^2 \frac{f(E, \theta)\cos(\theta)}{\sqrt{2E}} + \varepsilon \frac{g_1(t, E, \theta)\cos(\theta)}{\sqrt{2E}} + \frac{g(E, \theta)}{\sqrt{2E}\cos(\theta)} \end{aligned} \tag{34}$$

It can be seen from (31) that for the unperturbed system ($\varepsilon = 0$), energy E is independent of time. With the introduction of damping and parametric excitation, energy now varies slowly with time. This property of $E(t)$ enables the application of stochastic averaging that allows the energy to be approximated as a Markov process.

Introducing the phase angle $\theta_0(t)$ for the unperturbed case defined by

$$\theta_0 = \int \frac{g(E, \theta)}{\sqrt{2E}\cos(\theta)} dt \tag{35}$$

and defining a new phase process $\lambda(t)$ defined by

$$\lambda = \theta - \theta_0 \tag{36}$$

it can be seen that the governing equation for $\lambda(t)$ is given by

$$\dot{\lambda} = \varepsilon^2 \frac{f(E, \theta_0 + \lambda)\cos(\theta_0 + \lambda)}{\sqrt{2E}} + \varepsilon \frac{g_1(t, E, \theta_0 + \lambda)\cos(\theta_0 + \lambda)}{\sqrt{2E}} \tag{37}$$

This transformation is required to obtain a new phase process $\lambda(t)$ to achieve a vector process $\boldsymbol{Z}(t) = \begin{Bmatrix} E(t) \\ \lambda(t) \end{Bmatrix}$ that is slowly varying with time. The equation of motion for $\boldsymbol{Z}(t)$ is given by

$$\dot{\boldsymbol{Z}}(t) = \begin{bmatrix} \dot{E} \\ \dot{\lambda} \end{bmatrix} = \varepsilon^2 \boldsymbol{a}(\boldsymbol{Z}) + \varepsilon \boldsymbol{b}(t, \boldsymbol{Z}) \tag{38}$$

where

$$\boldsymbol{a}(\boldsymbol{Z}) = \begin{bmatrix} a_1(E, \theta) \\ a_2(E, \theta) \end{bmatrix} = \begin{bmatrix} f(E, \theta)\sqrt{2E}\sin(\theta) \\ \frac{f(E,\theta)\cos(\theta)}{\sqrt{2E}} \end{bmatrix} \tag{39}$$

$$\boldsymbol{b}(t, \boldsymbol{Z}) = \begin{bmatrix} b_1(t, E, \theta) \\ b_2(t, E, \theta) \end{bmatrix} = \begin{bmatrix} g_1(t, E, \theta)\sqrt{2E}\sin(\theta) \\ \frac{g_1(t,E,\theta)\cos(\theta)}{\sqrt{2E}} \end{bmatrix} \tag{40}$$

Since $g_1(t, E, \theta) = \sum_{j=1,3,5,...}^{2n_q-1} p_j(t) \left[x(E, \theta)\right]^j$, as shown in (25), the expression for $\boldsymbol{b}(t, \boldsymbol{Z})$ can be expanded as

$$\boldsymbol{b}(t, \boldsymbol{Z}) = \sum_{r=1,3,5,...}^{2n_q-1} \boldsymbol{d}_r(\boldsymbol{Z}) p_r(t) \tag{41}$$

where

$$\boldsymbol{d}_r(\boldsymbol{Z}) = \begin{bmatrix} d_{r1}(E, \theta) \\ d_{r2}(E, \theta) \end{bmatrix} = \begin{bmatrix} x^r(E, \theta)\sqrt{2E}\sin(\theta) \\ \frac{x^r(E,\theta)\cos(\theta)}{\sqrt{2E}} \end{bmatrix} \tag{42}$$

Thus the equation of motion for $\boldsymbol{Z}(t)$ is given by

$$\dot{\boldsymbol{Z}}(t) = \varepsilon^2 \boldsymbol{a}(\boldsymbol{Z}) + \varepsilon \sum_{r=1,3,5,...}^{2n_q-1} \boldsymbol{d}_r(\boldsymbol{Z}) p_r(t) \tag{43}$$

4. Approximation of a Real Process by a Markov Process

In general both the excitation $p_r(t)$ for $r = 1, 3, 5, ..., (2n_q - 1)$ and response $\boldsymbol{Z}(t)$ are not Markov processes. However, if the response $\boldsymbol{Z}(t)$ is approximated as a Markov process, it allows for further analysis using stochastic methods that are primarily applicable to Markov processes. With this motivation, we explore the conditions under which a real process can be approximated by a Markov process. Here we limit our discussions to heuristic arguments to better appreciate the physical significance behind the stochastic averaging technique and do not dwell too much into mathematical proofs. For a rigorous mathematical proof of stochastic averaging, readers are referred to the works of Khas'minskii [30], Papanicolau and Kohler [29].

The Markov process is a mathematical idealization and it is hard to find a physical process with similar properties. By definition of a Markov process, its increments in non-overlapping time increments are independent. Approximation of a real process by a Markov process is usually justified on the basis of how the close increments of the process in non-overlapping time intervals are nearly independent.

Let's assume that a continuous time process $\boldsymbol{Z}(t)$ is being observed at discrete time instants starting from t with intervals of $\Delta t_1, \Delta t_2, ...$ and the respective increments in the process over these time intervals be given by $\Delta \boldsymbol{Z}_1, \Delta \boldsymbol{Z}_2, ...$ If $\Delta \boldsymbol{Z}_1, \Delta \boldsymbol{Z}_2, ...$ are independent of each other regardless of how short $\Delta t_1, \Delta t_2, ...$ are (even as they approach zero that implies continuous time observation), then $\boldsymbol{Z}(t)$ satisfies the sufficient condition to be a Markov process. However, real processes rarely possess this property.

On the other hand, if the system response varies much more slowly than the excitation, then it is easy to appropriately choose these time gaps $\Delta t_1, \Delta t_2, ...$ such that they are much larger than the correlation time of excitation τ_{corr}. The correlation time τ_{corr} is a measure of the "memory" of the excitation of its earlier state. Lin and Cai [32] define the correlation time for two zero mean processes $r(u)$ and $s(v)$ as

$$\tau_{rs} = \frac{1}{\sqrt{w_{rr}(0) w_{ss}(0)}} \int_{-\infty}^{0} |w_{rs}(\tau)| d\tau \tag{44}$$

where covariance stationarity is assumed between them and the stationary covariance function is given by

$$w_{rs}(u - v) = E\left[r(u)s(v)\right] \tag{45}$$

If the time gaps $\Delta t_1, \Delta t_2, ...$ are chosen to be much larger than correlation time ($\Delta t_i >> \tau_{corr}$), the increments of the process $\Delta \boldsymbol{Z}_1, \Delta \boldsymbol{Z}_2, ...$ will appear independent. In such a scenario, if we choose to observe the process $\boldsymbol{Z}(t)$ at times that are separated by at least one correlation time τ_{corr} then the process will appear to have independent increments over non-overlapping time increments and may be approximated as a Markov process.

In our example of interest, roll x and roll velocity $\dot{x}$ fluctuate rapidly. However, the transformed coordinates - energy E and phase difference from unperturbed solution λ vary slowly on a much larger time scale as is evident from (43). Applying similar arguments as discussed above, $\boldsymbol{Z}(t)$ can be approximated as a diffusion. Mathematically, the Itô stochastic differential equation (SDE) governing the diffusion process can be expressed as (46)

$$d\boldsymbol{Z} = \boldsymbol{m}(\boldsymbol{Z})dt + \boldsymbol{\sigma}(\boldsymbol{Z})d\boldsymbol{B}_t \tag{46}$$

where $\boldsymbol{m}(\boldsymbol{Z})$ and $\boldsymbol{\sigma}(\boldsymbol{Z})$ are the drift and diffusion coefficients respectively and $\boldsymbol{B}_t$ represents the vector Brownian motion. Integrating (46) results in (47).

$$\Delta \boldsymbol{Z} = \boldsymbol{Z}_{t+\Delta t} - \boldsymbol{Z}_t = \int_t^{t+\Delta t} \boldsymbol{m}(\boldsymbol{Z}_u)du + \int_t^{t+\Delta t} \boldsymbol{\sigma}(\boldsymbol{Z}_u)d\boldsymbol{B}_u \tag{47}$$

Heuristically, for a sufficiently small Δt in (47), $\Delta \boldsymbol{Z}$ may be thought of as a normally distributed random variable with mean vector $\boldsymbol{m}(\boldsymbol{Z}_t)\Delta t$ and covariance matrix $\boldsymbol{\sigma}(\boldsymbol{Z}_t)\boldsymbol{\sigma}^T(\boldsymbol{Z}_t)\Delta t$. The transition probability density of $\boldsymbol{Z}(t)$, given by $p(\boldsymbol{z}, t|\boldsymbol{z}_0, t_0)$, is governed by the FPK equation given by

$$\begin{aligned} \frac{\partial p}{\partial t} = & -\sum_{i=1}^{2} \frac{\partial}{\partial z_i}\left[m_i(\boldsymbol{Z})p(\boldsymbol{z}, t|\boldsymbol{z}_0, t_0)\right] \\ & + \frac{1}{2}\sum_{i=1}^{2}\sum_{j=1}^{2} \frac{\partial^2}{\partial z_i \partial z_j}\left[D_{ij}(\boldsymbol{Z})p(\boldsymbol{z}, t|\boldsymbol{z}_0, t_0)\right] \end{aligned} \tag{48}$$

where $\boldsymbol{D} = \boldsymbol{\sigma}\boldsymbol{\sigma}^T$.

The drift $\boldsymbol{m}(\boldsymbol{Z})$ and diffusion $\boldsymbol{D}(\boldsymbol{Z})$ coefficients of the approximated Markov process $\boldsymbol{Z}(t)$ are obtained from the equation governing the physical process (38) by the application of Stratonovich-Khas'minskii limit theorem. The Stratonovich-Khas'minskii theorem embodies the mathematical rigor involved with the heuristic argument developed above. The proof of this theorem can be found in the works of Khas'minskii [30] and Papanicolau and Kohler [29]. The resulting expressions for the drift and diffusion coefficients from the application of this theorem are given by (49) and (50) respectively

$$\boldsymbol{m} = \boldsymbol{A}(E) + \int_{-\infty}^{0} \left\langle E\left[\left(\frac{\partial \boldsymbol{b}}{\partial \boldsymbol{Z}}\right)_t (\boldsymbol{b})_{t+\tau}\right]\right\rangle d\tau \tag{49}$$

$$\boldsymbol{D} = \boldsymbol{\sigma}\boldsymbol{\sigma}^T = \int_{-\infty}^{\infty} \left\langle E\left[(\boldsymbol{b})_t\, (\boldsymbol{b})_{t+\tau}^T\right]\right\rangle d\tau \tag{50}$$

where $\boldsymbol{a}(\boldsymbol{Z})$ and $\boldsymbol{b}(t, \boldsymbol{Z})$ are as defined in (39) and (40) respectively and

$$\frac{\partial \boldsymbol{b}}{\partial \boldsymbol{Z}} = \begin{bmatrix} \frac{\partial b_1}{\partial E} & \frac{\partial b_1}{\partial \lambda} \\ \frac{\partial b_2}{\partial E} & \frac{\partial b_2}{\partial \lambda} \end{bmatrix} \tag{51}$$

$$\boldsymbol{A}(E) = \begin{bmatrix} A_1(E) \\ A_2(E) \end{bmatrix} = \langle \boldsymbol{a}(E, \theta_0)\rangle = \frac{1}{T(E)} \int_0^{T(E)} \boldsymbol{a}(E, \theta_0)dt \tag{52}$$

and $\langle[.]\rangle$ denotes the time average over the period of the unperturbed system $T(E)$ and is given by

$$\langle[\ .\ ]\rangle = \frac{1}{T(E)} \int_0^{T(E)} [\ .\ ]dt \tag{53}$$

where the unperturbed system period $T(E)$ is given by

$$T(E) = \oint \left|\frac{dx}{\dot{x}}\right| = 4\int_0^b \frac{dx}{\sqrt{2E}\sin(\theta)} = 2\sqrt{2}\int_0^b \frac{dx}{\sqrt{E - U(x)}} \tag{54}$$

where b is the maximum displacement along the path of the unperturbed system about which the averaging is performed. Substitution of (39) and (40) into (49) and (50) results in the following expressions for the drift and diffusion coefficients.

$$\begin{aligned} m_1 =& A_1(E) + \sum_{j=1,3,5,\ldots}^{2n_q-1} \sum_{k=1,3,5,\ldots}^{2n_q-1} \left[\left(\int_{-\infty}^{0} w_{jk}(\tau)d\tau\right)\left\{a_0^{(1j)}a_0^{(1k)} + a_0^{(2j)}a_0^{(1k)}\right\}\right. \\ &+ \sum_{n=1}^{\infty}\left(\int_{-\infty}^{0} w_{jk}(\tau)\cos\left(\frac{2\pi n}{T(E)}\tau\right)d\tau\right) \\ &\left.\times\left\{\frac{b_n^{(1j)}b_n^{(1k)}}{2} + \frac{a_n^{(1j)}a_n^{(1k)}}{2} + (j)\frac{b_n^{(2j)}b_n^{(1k)}}{2} + (j)\frac{a_n^{(2j)}a_n^{(1k)}}{2}\right\}\right] \end{aligned} \tag{55}$$

$$\begin{aligned} m_2 =& A_2(E) + \sum_{n=1}^{\infty} \sum_{j=1,3,5,\ldots}^{2n_q-1} \sum_{k=1,3,5,\ldots}^{2n_q-1} \left[\left(\int_{-\infty}^{0} w_{jk}(\tau)\sin\left(\frac{2\pi n}{T(E)}\tau\right)d\tau\right)\right. \\ &\left.\times\left\{-\frac{a_n^{(1j)}b_n^{(1k)}}{4E} + \frac{b_n^{(1j)}a_n^{(1k)}}{4E} + (j)\frac{d_n^{(2j)}b_n^{(1k)}}{2} + (j)\frac{b_n^{(2j)}a_n^{(1k)}}{4E}\right\}\right] \end{aligned} \tag{56}$$

$$D_{11} = \sum_{n=1}^{\infty} \sum_{j=1,3,5,\ldots}^{2n_q-1} \sum_{k=1,3,5,\ldots}^{2n_q-1} \left[(2\pi E) \left\{ b_n^{(1j)} b_n^{(1k)} \right\} S_{jk}^{(c)} \left(\frac{2\pi n}{T(E)} \right) \right] \tag{57}$$

$$D_{12} = \sum_{n=1}^{\infty} \sum_{j=1,3,5,\ldots}^{2n_q-1} \sum_{k=1,3,5,\ldots}^{2n_q-1} \left[-\pi b_n^{(1j)} a_n^{(1k)} S_{jk}^{(s)} \left(\frac{2\pi n}{T(E)} \right) \right] \tag{58}$$

$$D_{21} = \sum_{n=1}^{\infty} \sum_{j=1,3,5,\ldots}^{2n_q-1} \sum_{k=1,3,5,\ldots}^{2n_q-1} \left[\pi a_n^{(1j)} b_n^{(1k)} S_{jk}^{(s)} \left(\frac{2\pi n}{T(E)} \right) \right] \tag{59}$$

$$D_{22} = \sum_{j=1,3,5,\ldots}^{2n_q-1} \sum_{k=1,3,5,\ldots}^{2n_q-1} \left[\frac{\pi}{E} \left\{ a_0^{(1j)} a_0^{(1k)} \right\} S_{jk}^{(c)}(0) + \sum_{n=1}^{\infty} \frac{\pi}{2E} \left\{ a_n^{(1j)} a_n^{(1k)} \right\} S_{jk}^{(c)} \left(\frac{2\pi n}{T(E)} \right) \right] \tag{60}$$

where $a_n^{(1k)}$, $b_n^{(1k)}$, $a_n^{(2k)}$, $b_n^{(2k)}$ and $d_n^{(2k)}$ are Fourier series coefficients and satisfy the following equations:

$$\sin(\theta_0(t)) x_0^k(t) = \sum_{n=1}^{\infty} b_n^{(1k)} \sin\left(\frac{2\pi n}{T(E)} t \right) \tag{61}$$

$$\cos(\theta_0(t)) x_0^k(t) = a_0^{(1k)} + \sum_{n=1}^{\infty} a_n^{(1k)} \cos\left(\frac{2\pi n}{T(E)} t \right) \tag{62}$$

$$\frac{2E}{g(E,\theta_0(t))} \sin(\theta_0(t)) \cos^2(\theta_0(t)) x_0^{k-1}(t) = \sum_{n=1}^{\infty} b_n^{(2k)} \sin\left(\frac{2\pi n}{T(E)} t \right) \tag{63}$$

$$\frac{2E}{g(E,\theta_0(t))} \sin^2(\theta_0(t)) \cos(\theta_0(t)) x_0^{k-1}(t) = a_0^{(2k)} + \sum_{n=1}^{\infty} a_n^{(2k)} \cos\left(\frac{2\pi n}{T(E)} t \right) \tag{64}$$

$$\frac{\cos^3 \theta_0(t)}{g(E,\theta_0(t))} x_0^{k-1}(t) = d_0^{(2k)} + \sum_{n=1}^{\infty} d_n^{(2k)} \cos\left(\frac{2\pi n}{T(E)} t \right) \tag{65}$$

where $\theta_0(t)$ and $x_0(t)$ are the solutions of the unperturbed system. The cosine and sine cross spectra $S_{jk}^{(c)}(\omega)$ and $S_{jk}^{(s)}(\omega)$ are defined as

$$S_{jk}^{(c)}(\omega) = \frac{1}{2\pi} \int_{-\infty}^{\infty} w_{jk}(\tau) \cos(\omega\tau)\, d\tau \tag{66}$$

$$S_{jk}^{(s)}(\omega) = \frac{1}{2\pi} \int_{-\infty}^{\infty} w_{jk}(\tau) \sin(\omega\tau)\, d\tau \tag{67}$$

where $w_{jk}(\tau) = E\left[p_j(t) p_k(t+\tau) \right]$. The drift and the diffusion coefficients of the energy equation computed using (55), (57) and (58) are shown in Figure 6a and Figure 6b respectively.

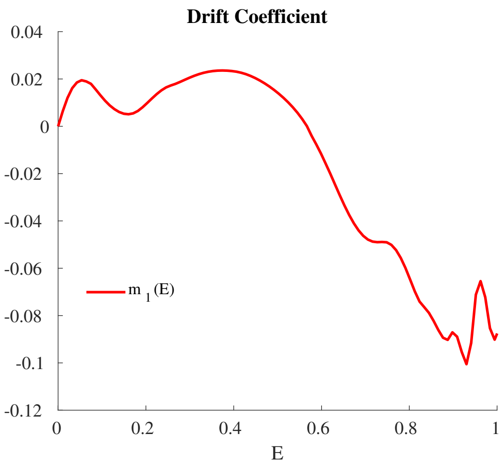

(a) $m_1(E)$

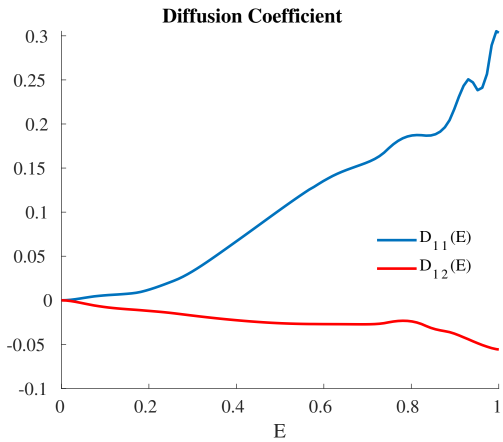

(b) $D_{11}(E)$ and $D_{12}(E)$

Figure 6: Drift coefficient $m_1(E)$ and diffusion coefficients $D_{11}(E)$ and $D_{12}(E)$ for $H_s = 8.0\ m$, $T_p = 13.0\ s$ and $\beta = 180^0$

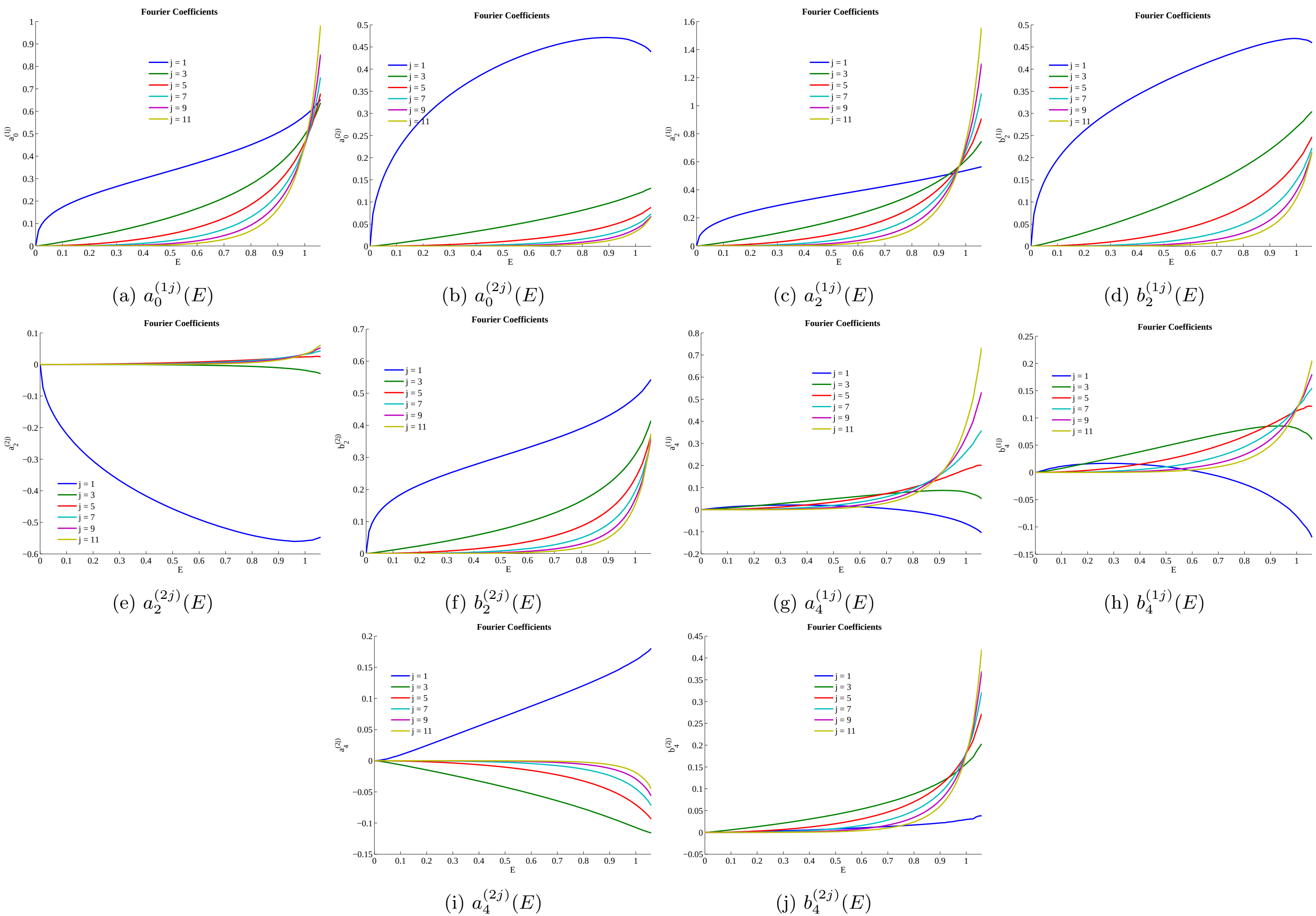

(a) $a_0^{(1j)}(E)$ (b) $a_0^{(2j)}(E)$ (c) $a_2^{(1j)}(E)$ (d) $b_2^{(1j)}(E)$

(e) $a_2^{(2j)}(E)$ (f) $b_2^{(2j)}(E)$ (g) $a_4^{(1j)}(E)$ (h) $b_4^{(1j)}(E)$

(i) $a_4^{(2j)}(E)$ (j) $b_4^{(2j)}(E)$

Figure 7: Plot of $a_n^{(1j)}(E)$, $b_n^{(1j)}(E)$, $a_n^{(2j)}(E)$ and $b_n^{(2j)}(E)$ for $n = 0, 2, 4$

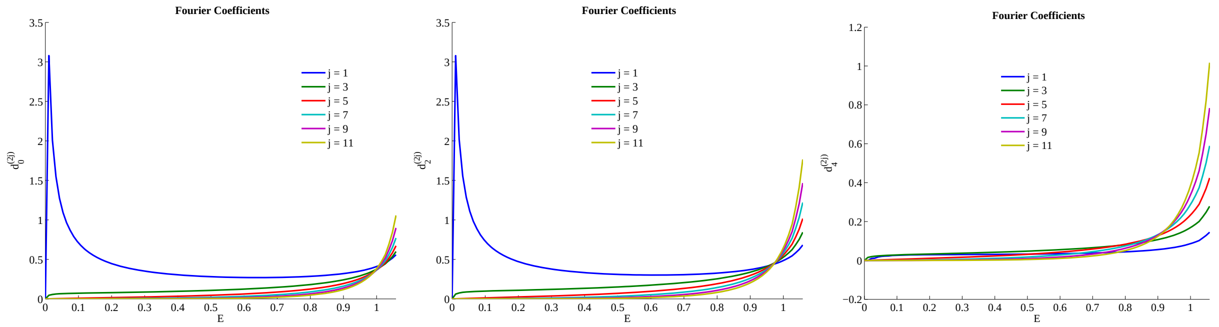

(a) $d_0^{(2j)}(E)$ (b) $d_2^{(2j)}(E)$ (c) $d_4^{(2j)}(E)$

Figure 8: Plot of $d_n^{(2j)}(E)$ for $n = 0, 2, 4$

Since $x_0(t)$ has a periodicity similar to $\cos(\theta_0(t))$, substituting it into (61-65) results in non-zero values for $b_n^{(1j)}(E)$, $a_n^{(1j)}(E)$, $b_n^{(2j)}(E)$, $a_n^{(2j)}(E)$ and $d_n^{(2j)}(E)$ only when n is even. The non-zero Fourier coefficients are shown in Figure 7 and Figure 8.

So far we have shown that $\boldsymbol{Z}(t)$ can be approximated as a two dimensional Markov process. It can be observed from Figure 6b that the cross diffusion term $D_{12}(E)$ is much smaller than the main term $D_{11}(E)$. In this study we neglect the smaller cross diffusion term and approximate the energy as a Markov process governed by (68) where $\sigma_{11}(E) = \sqrt{D_{11}(E)}$.

$$dE = m_1(E)dt + \sigma_{11}(E)dB_t \tag{68}$$

Figure 9a and Figure 9b show the variation of drift and diffusion coefficients of the energy equation for different Bretschneider spectra with varying significant wave heights and constant peak period $T_p = 13.0\ s$. It can be seen that the drift and diffusion coefficients vary monotonically with significant wave height. Figure 10a and Figure 10b show the variation of drift and diffusion coefficients of the energy equation for different Bretschneider spectra with varying peak periods and constant significant wave height $H_s = 8.0\ m$.

5. Stationary Probability Density Function

Once the drift and diffusion coefficients for the energy equation are known, the transition probability density function can be obtained by solving the corresponding FPK equation given by

$$\frac{\partial p}{\partial t} = -\frac{\partial}{\partial E}\left[m_1(E)p(E,t|E_0,t_0)\right] + \frac{1}{2}\frac{\partial^2}{\partial E^2}\left[D_{11}(E)p(E,t|E_0,t_0)\right] \tag{69}$$

If stationarity is assumed, the FPK equation reduces to an ordinary differential equation given by

$$\frac{dp}{dE} + \frac{1}{D_{11}}\left[\frac{dD_{11}}{dE} - 2m_1\right]p = 0 \tag{70}$$

and the solution is given by (71)

$$p(E) = K_1 \exp\left\{-\int_0^E \frac{1}{D_{11}(s)}\left[\frac{dD_{11}}{ds}(s) - 2m_1(s)\right]ds\right\} \tag{71}$$

where K_1 is a normalization constant chosen such that

$$\int_0^\infty p(E)dE = 1 \tag{72}$$

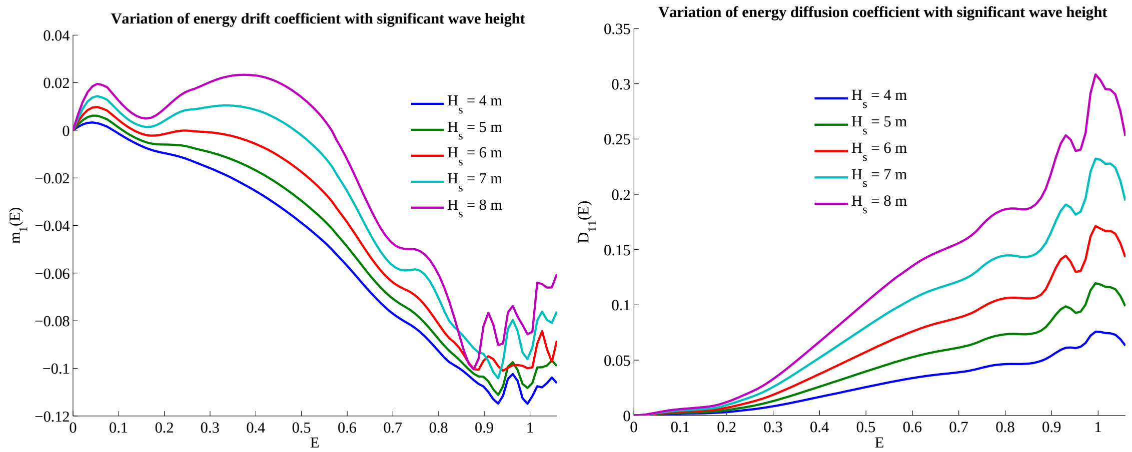

(a) Energy drift coefficient

(b) Energy diffusion coefficient

Figure 9: Energy drift and diffusion coefficients for various H_s and a fixed chosen $T_p = 13.0\ s$

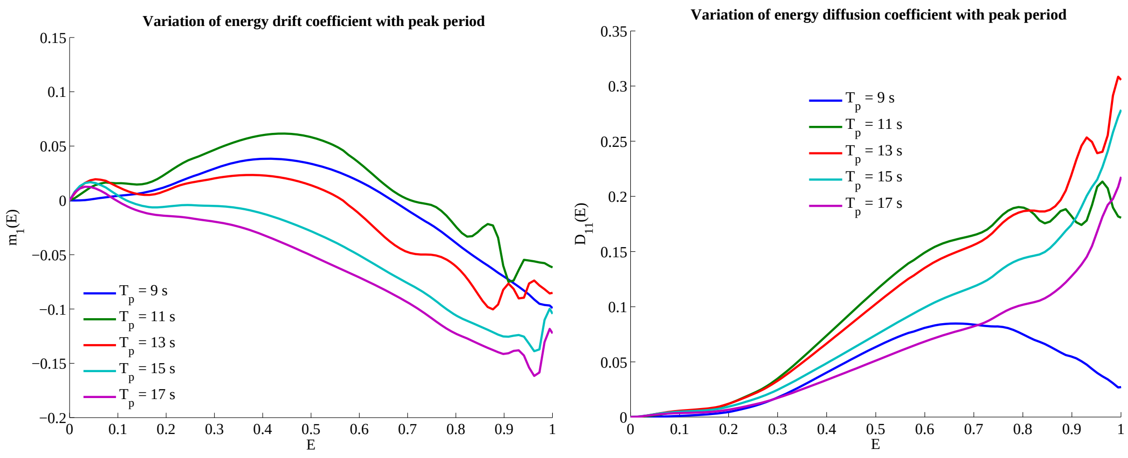

(a) Energy drift coefficient

(b) Energy diffusion coefficient

Figure 10: Energy drift and diffusion coefficients for various T_p and a fixed chosen $H_s = 8.0\ m$

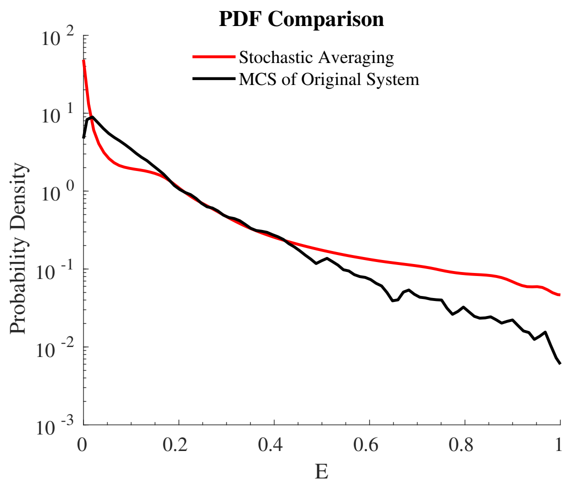

(a) Stationary PDF

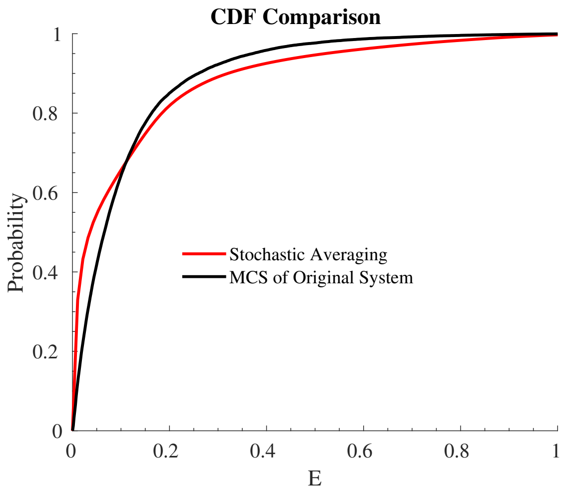

(b) Stationary CDF

Figure 11: Stationary probability and cumulative distribution functions of energy E for $H_s = 8.0\ m$ and $T_p = 13.0\ s$

Figure 11a and Figure 11b show the stationary probability density function and cumulative distribution function of the energy for the case of incident wave environment with $H_s = 8.0\ m$ and $T_p = 13.0\ s$ incident at angle $\beta = 180^0$. The probability density function and cumulative distribution function from Monte Carlo simulations of the original system given by (11) are also plotted for comparison. It can be seen that the estimates from stochastic averaging are in agreement with simulations at lower energy levels and tend to exponential behaviour at higher energy levels. The rate of exponential decay for the original system is much higher than that for the averaged system. This means that the averaged process is more likely to reach the capsize boundary, as compared to the original system. This idea will be further investigated in the next section using first passage statistics.

6. First Passage Failure Analysis

The analysis of section 5 focused on determining the probability density function of the energy of a stationary response. Although this information is useful, it does not meet an important need of the ship designer. In particular, a designer is usually more interested in the probability that the energy of the system will exceed a critical value within some specified period of time. This problem is classically referred to as the first passage failure analysis. The mean first passage time is indicative of the stability of the system and hence can be used as a design assessment metric to compare different systems. Similarly the standard deviation of the first passage time gives information about the uncertainty of the assessment metric.

Consider the decoupled Itô equation for the energy process given by (68). Specifically, we are interested in the random time τ_{FP} when the scalar energy process $E(t)$ exceeds a critical value E_c given that the system starts from an initial energy level of E_0 at time t_0. Assuming that the transition probability density function for the energy process is given by $p(E, t|E_0, t_0)$, it is possible to define a reliability function $R(E_c, t|E_0, t_0)$ that denotes the probability of $0 \leq E(t) < E_c$. The reliability function $R(E_c, t|E_0, t_0)$ is mathematically defined as

$$R(E_c, t|E_0, t_0) = \int_0^{E_c} p(E, t|E_0, t_0)dE \tag{73}$$

It is further assumed that the boundary at $E = E_c$ is an absorbing boundary. This implies that a sample path is removed from the population of sample paths once it reaches the boundary $E = E_c$. Without this assumption of absorbing boundary condition, the population of sample paths can include a sample path that exceeds E_c and at a later time goes below E_c. In such a scenario, it is particularly hard to calculate the mean first passage time as it needs to be ensured that the process has never exceeded the boundary before the considered first passage time. However, in the problem of parametric roll, the boundary $E = E_c$ corresponds to the energy level at the tipping point beyond which capsize results. Considering $E = E_c$ as an absorbing boundary is equivalent to saying that the energy process $E(t)$ can never achieve a value of E_c without resulting in capsize. Since the population of sample paths at time t only include those paths that have not crossed E_c even once, the reliability function defined above is also equal to the probability that the first passage time $\tau_{FP} > t - t_0$.

$$R(E_c, t|E_0, t_0) = \int_0^{E_c} p(E, t|E_0, t_0)dE = \text{Prob}\left[\tau_{FP} > t - t_0 | E(t_0) = E_0\right] \tag{74}$$

With an absorbing boundary condition, the process can never attain stationarity. This also implies that the probability in the region $0 \le E \le E_c$ is not conserved as otherwise the reliability function would be unity. Since $p(E, t|E_0, t_0)$ satisfies the Kolmogorov backward equation, the reliability function R will also satisfy the same.

$$\frac{\partial R}{\partial t_0} + m_1(E_0)\frac{\partial R}{\partial E_0} + \frac{1}{2}D_{11}(E_0)\frac{\partial^2 R}{\partial E_0^2} = 0 \tag{75}$$

Defining a change of variable $\tau = t - t_0$, (75) can be expressed as

$$-\frac{\partial R}{\partial \tau} + m_1(E_0)\frac{\partial R}{\partial E_0} + \frac{1}{2}D_{11}(E_0)\frac{\partial^2 R}{\partial E_0^2} = 0 \tag{76}$$

The cumulative probability distribution function of the first passage time τ_{FP} is given by

$$F_{\tau_{FP}}(\tau, E_c, E_0) = \text{Prob}\left[\tau_{FP} \le \tau | E(t_0) = E_0\right] \tag{77}$$
$$= 1 - R(\tau, E_c, E_0) \tag{78}$$

The probability density function of τ_{FP} is given by

$$p_{\tau_{FP}}(\tau, E_c, E_0) = \frac{\partial F_{\tau_{FP}}}{\partial \tau}(\tau, E_c, E_0) = -\frac{\partial R}{\partial \tau}(\tau, E_c, E_0) \tag{79}$$

Thus, the n^{th} moment of τ_{FP} is given by

$$\mu_n(E_c, E_0) = E\left[\tau_{FP}^n\right] = -\int_0^\infty \tau^n \frac{\partial R}{\partial \tau}(\tau, E_c, E_0)d\tau \tag{80}$$

Assuming $\tau^n R(\tau, E_c, E_0)$ tends to zero as $\tau \to 0$, $\mu_n(E_c, E_0)$ can be expressed as

$$\mu_n(E_c, E_0) = n\int_0^\infty \tau^{n-1} R(\tau, E_c, E_0)d\tau \tag{81}$$

Multiplying (76) by τ^n and integrating with respect to τ from 0 to ∞ results in a recursive set of ordinary differential equations for the moments of τ_{FP}.

$$n\mu_{n-1} + m_1(E_0)\frac{d}{dE_0}\mu_n + \frac{1}{2}D_{11}(E_0)\frac{d^2}{dE_0^2}\mu_n = 0 \tag{82}$$

These set of equations shown in (82) are known as generalized Pontryagin equations and can be solved recursively. Substituting $n = 1$ and $\mu_0 = 1$ leads to Pontryagin equation governing the mean first passage time $\mu_1 = E\left[\tau_{FP}\right]$ given by (83).

$$1 + m_1(E_0)\frac{d\mu_1}{dE_0} + \frac{1}{2}D_{11}(E_0)\frac{d^2\mu_1}{dE_0^2} = 0 \tag{83}$$

The boundary conditions for (83) are given by

$$\mu_1(E_c, E_0)|_{E_0=E_c} = 0 \tag{84}$$

$$\mu_1(E_c, E_0)|_{E_0=0} < \infty \tag{85}$$

Many of the steps of the derivation of the Pontryagin equation provided above follow the works of Lin and Cai [32] and have been summarized here for completeness. Note that the derivation of the Pontryagin equation does not assume that the process is stationary.

The second boundary condition shown in (85) physically signifies that given enough time, the system will eventually reach the critical boundary. This condition is "qualitative" rather than "quantitative", and is only useful when closed form solutions exist. In many of the practical cases where closed form solutions do not exist, (83) is solved numerically to obtain estimates of $\mu_1(E_c, E_0)$. In such cases, it is necessary to convert the boundary condition shown in (85) into a quantitative condition that can be applied numerically. This conversion from a qualitative to a quantitative condition is discussed next.

6.1. Boundary Condition at $E = 0$

According to Feller [59], the boundaries of a diffusion process can be classified as follows:

1. *Regular boundary*: The process can reach the boundary starting from an interior point and also can reach an interior point starting from the boundary
2. *Absorbing/Exit boundary*: The process can reach the boundary starting from an interior point but cannot reach an interior point starting from the boundary
3. *Entrance boundary*: The process can reach an interior point starting from the boundary but cannot reach the boundary starting from an interior point
4. *Natural boundary*: The process cannot reach the boundary starting from an interior point and also cannot reach an interior point starting from the boundary. Lin and Cai [32] further specify a sub-classification of natural boundary into strictly natural, attractively natural and repulsively natural boundary types depending on the behavior of the system close to boundary.

Often various conclusions about the existence of a stationary transition probability density function or an eventual inevitable escape through a critical boundary can be drawn based on the type of boundaries. In general, the type of boundary can be mathematically ascertained [32]. However, for certain special types of boundaries called the singular boundaries, the above approach is not applicable and requires special consideration. A boundary at $E = E_b$ of a diffusion process $E(t)$ is defined to be singular if at the boundary either of the following hold:

1. Diffusion coefficient is zero at the boundary ($D_{11}(E_b) = \sigma_{11}^2(E_b) = 0$). This type of a boundary is known as singular boundary of first kind.
2. Drift coefficient at the boundary is unbounded ($m_1(E_b) \to \pm\infty$). This type of a boundary is known as singular boundary of second kind.

Further, a singular boundary of first kind is called a *trap* if the drift coefficient at the boundary is also zero. A singular boundary of first kind with a non-zero drift coefficient at the boundary is called a *shunt*. From Figure 9b and Figure 10b it can be seen that the diffusion coefficient $D_{11}(E)$ at $E = 0$ is zero. Thus for the Markov energy process $E(t)$ considered in (68) the boundary $E = 0$ is a singular boundary of the first kind. From Figure 9a and Figure 10a it can further be seen that the boundary at $E = 0$ is a trap as the drift coefficient at $E = 0$ is zero.

To determine the Feller classification of a singular boundary of the first kind, the following definitions are introduced as $E \to E_b$ where $E = E_b$ is the singular boundary under consideration:

1. *Diffusion exponent* α_b where $\sigma_{11}^2(E) = O(|E - E_b|^{\alpha_b})$ as $E \to E_b$

2. *Drift exponent* β_b where $m_1(E) = O(|E - E_b|^{\beta_b})$ as $E \to E_b$

3. *Character value* c_b where $c_b = \frac{2m_1(E)(E-E_b)^{\alpha_b - \beta_b}}{\sigma_{11}^2(E)}$ as $E \to E_b$

A table indicating the Feller classification of the singular boundaries of first kind based on the values of the drift exponent, diffusion exponent and the character value is provided by Lin and Cai [32]. Lin and Cai [32] argue that if the left boundary (in this case at $E = 0$) is either an exit, attractively or strictly natural, then not every sample path starting near this boundary is capable of reaching the critical boundary (in this case at $E = E_c$). However, if the left boundary is an entrance, regular or a repulsively natural boundary, then every sample path starting near this boundary is capable of reaching the critical boundary. Thus for parametric roll system which has a trap at $E = 0$, a solution of the Pontryagin equation is possible only if the trap boundary is of type regular, entrance or repulsively natural. For these cases, the boundary condition can be expressed as shown in (86) [60].

$$m_1(E_0)\mu_1'(E_0) < \infty \text{ as } E_0 \to 0 \tag{86}$$

It can further be shown that for ship roll system, $E = 0$ corresponds to a natural type of trap (see Appendix A for details) with diffusion exponent $\alpha_0 = 2$ and drift exponent $\beta_0 = 1$ and character value c_0 given by (87).

$$c_0 = 2\left(1 - \frac{\delta_1}{\pi S_{11}^{(c)}(2)}\right) \tag{87}$$

Based on the character value c_0, the natural trap at $E = 0$ can further be characterized as either a strictly natural trap ($c_0 = 1$), an attractively natural trap ($c_0 < 1$) or a repulsively natural trap ($c_0 > 1$). Only when $c_0 > 1$, the boundary is a repulsively natural trap and the system is vulnerable to parametric response and a possible capsizing may occur. This vulnerability condition can be further simplified as

$$\delta_1 < \frac{\pi S_{11}^{(c)}(2)}{2} \tag{88}$$

When the linear damping in the system is low compared to excitation, the system is vulnerable to parametric response. Ideally a ship designer would want the linear damping to be sufficiently high so that (88) is never satisfied. However, this might not be possible for certain sea states, in which case the vulnerability can be quantified in terms of the mean first passage time obtained by solving the Pontryagin equation. A quantitative mathematical boundary condition for numerically solving the boundary value problem is obtained by linearizing the system about the boundary.

As $E \to 0$ the nonlinear oscillator can be approximated using only the linear damping and linear restoring terms. The drift and diffusion coefficients for this linear oscillator are obtained using stochastic averaging. The corresponding Pontryagin equation for the linear oscillator is solved to obtain an analytical expression for $\mu_1'(E_0)$ near $E_c = 0$. Applying this technique to the Volterra $\overline{GZ}$ model, leads to boundary condition given by (89). Detailed derivation of the drift and diffusion coefficients for the linear system and the boundary condition for the singular boundary at $E = 0$ are provided in Appendix A.

$$E_0\mu_1'(E_0) = \frac{-2}{\pi S_{11}^c(2) - 2\delta_1} < \infty \tag{89}$$

Adopting a similar procedure for mean squared first passage time μ_2 results in the boundary condition given by (90).

$$E_0\mu_2'(E_0) = \frac{8\left[\left(1 - \frac{2\delta_1}{\pi S_{11}^c(2)}\right)\ln(E) - 1\right]}{\left(\pi S_{11}^{(c)}(2) - 2\delta_1\right)^2\left(1 - \frac{2\delta_1}{\pi S_{11}^c(2)}\right)} \tag{90}$$

Note that although (89) and (90) provide quantitative conditions, they cannot be applied exactly at $E = 0$ when attempting a direct numerical solution of the Pontryagin equation. Instead this boundary condition is applied at a point slightly away from $E = 0$.

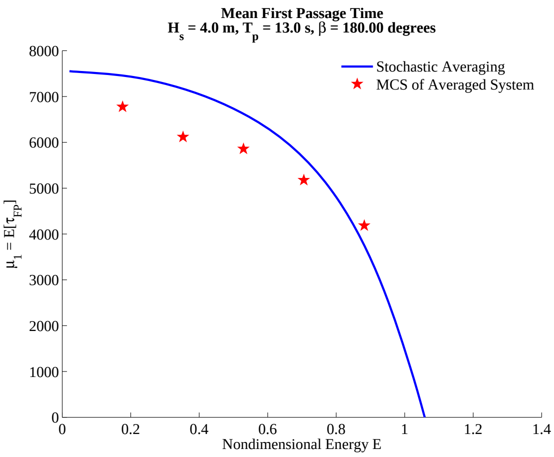

(a) $H_s = 4.0m$, Character value $c_0 = 1.9085$

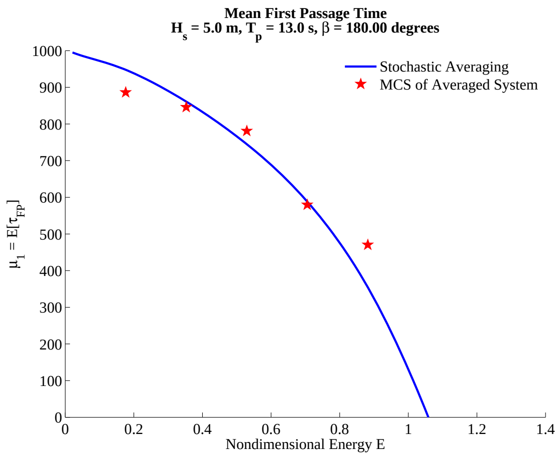

(b) $H_s = 5.0m$, Character value $c_0 = 1.9415$

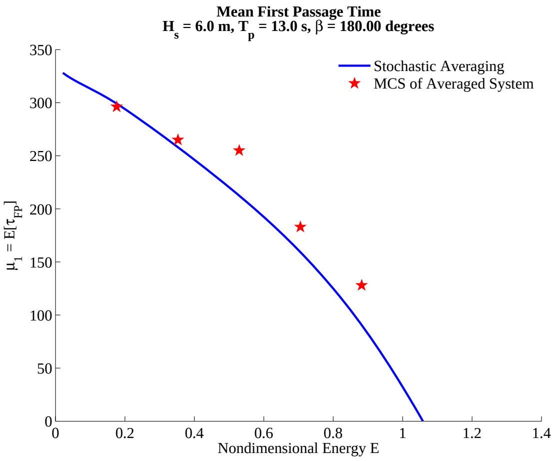

(c) $H_s = 6.0m$, Character value $c_0 = 1.9596$

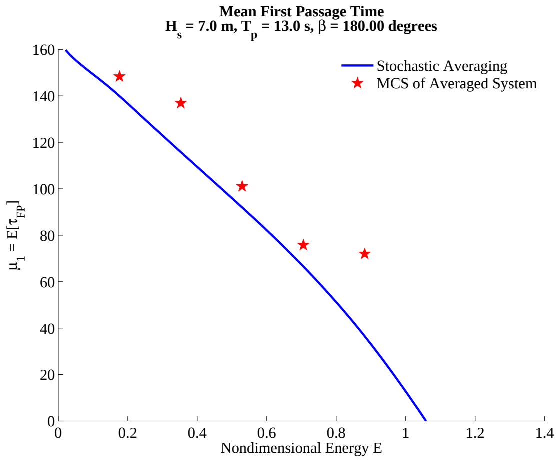

(d) $H_s = 7.0m$, Character value $c_0 = 1.9700$

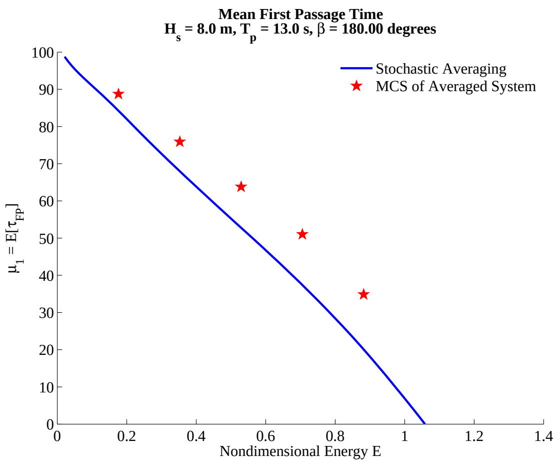

(e) $H_s = 8.0m$, Character value $c_0 = 1.9772$

Figure 12: Comparison of mean first passage times calculated from stochastic averaging and Monte Carlo simulations for different significant wave heights and fixed peak period $T_p = 13.0$ *sec*. The x-axis denotes the nondimensional initial energy of the system.

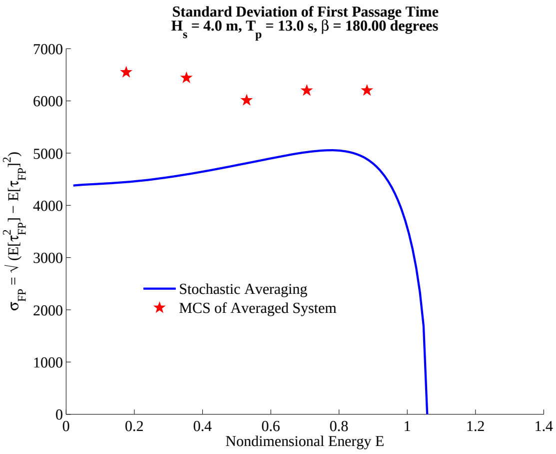

(a) $H_s = 4.0m$, Character value $c_0 = 1.9085$

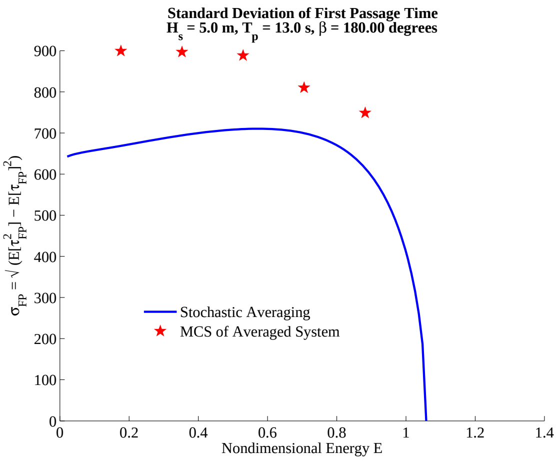

(b) $H_s = 5.0m$, Character value $c_0 = 1.9415$

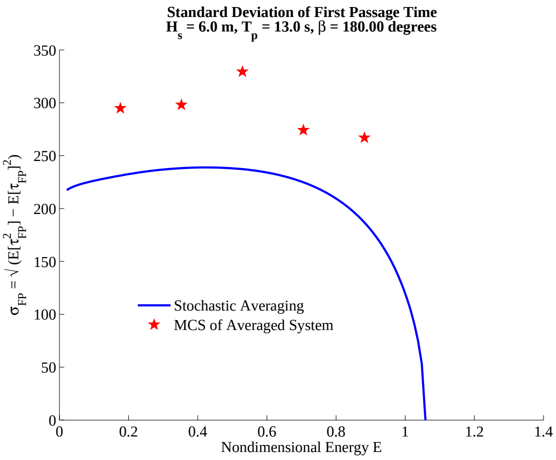

(c) $H_s = 6.0m$, Character value $c_0 = 1.9596$

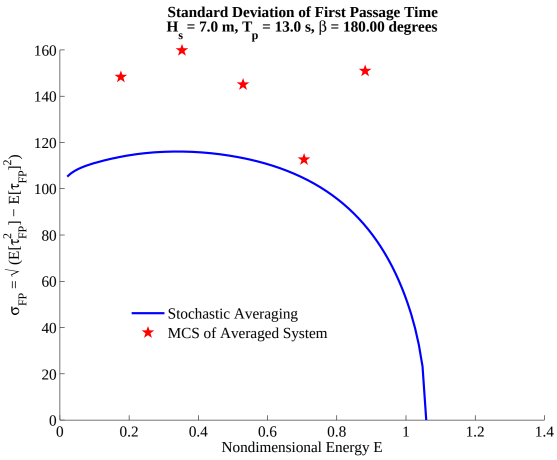

(d) $H_s = 7.0m$, Character value $c_0 = 1.9700$

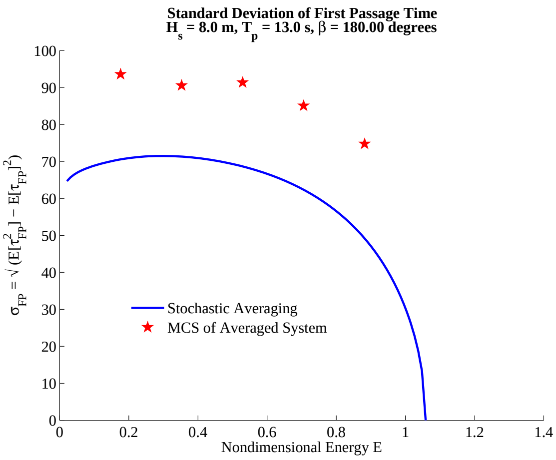

(e) $H_s = 8.0m$, Character value $c_0 = 1.9772$

Figure 13: Comparison of standard deviation of first passage times calculated from stochastic averaging and Monte Carlo simulations for different significant wave heights and fixed peak period $T_p = 13.0$ *sec*. The x-axis denotes the nondimensional initial energy of the system.

7. Comparison with Monte Carlo Simulations

In order to check the validity of the developed theory, the obtained mean first passage times are compared against estimates from Monte Carlo simulations of both the "*averaged system*" and the "*original system*". The original system refers to the non-dimensional equation of motion describing the dynamics of roll motion of a vessel and is given by (11). The averaged system refers to the Itô SDE obtained after stochastically averaging the original system over one cycle of response and is shown in (68).

7.1. Averaged System Monte Carlo Simulations

As the Itô SDE in (68) contains an excitation term proportional to increments of Brownian motion, every realization will eventually reach the boundary E_c, but this could occur for a very large value of time. For this reason, it is desirable to use a rather large finite simulation time for a Monte Carlo investigation. In this study the simulation time was chosen as approximately 10 times the mean crossing time from the Pontryagin equation (i.e. $T_{max} \approx 10(\mu_1)_{E_0=0}$), which was found to be quite adequate, since all simulation time histories did reach first passage. For a set of significant wave heights ($H_s = 4\ m,\ 5\ m,\ 6\ m,\ 7\ m,\ 8\ m$) and peak period $T_p = 13\ sec$, five equally spaced initial energy levels are chosen between 0 and E_c for each case. 1000 simulations are performed for every initial energy level within each case.

The mean Monte Carlo first passage time for a given initial energy level and a significant wave height is calculated as the average of the crossing times of the 1000 simulations corresponding to that initial energy and significant wave height. The governing Itô SDE shown in (68) is used to simulate the energy process. The Milstein scheme described by Higham [61] is used to simulate the Itô SDE. Figure 12 shows the mean first passage time μ_1 versus the non-dimensional initial energy level E for various values of the significant wave height H_s, but all with head seas ($\beta = 180^0$) and the same value of the wave peak period $T_p = 13.0\ sec$. The plot shows the comparison of the mean first passage times obtained from solving the Pontryagin equation against the estimates from Monte Carlo simulations of Itô SDE. It can be seen that the mean first passage times found by solving the Pontryagin equation agree well with those calculated from simulations. The slight deviation between the theory and the Monte Carlo simulations at higher energy levels indicate that the solution of the Pontryagin equation is more conservative in the estimation of mean first passage time. This implies that if a designer utilizes this approach, the designed system will be at least as stable or even more stable than if the designer had utilized the simulation approach to estimate the mean first passage time for the averaged system.

A similar comparison for standard deviation of first passage times is shown in Figure 13. The standard deviation of first passage time obtained by solving the Pontryagin equation agrees in trend with that calculated from Monte Carlo simulations. However, the estimates from simulations are consistently higher indicating a wider spread.

7.2. Original System Monte Carlo Simulations

When performing the Monte Carlo simulations of the original system given by (11), it is important to transform the specified initial energy into appropriate initial conditions. Note that the energy level is specified prior to the simulation. However the phase angle θ is chosen from a uniformly distributed random variable varying between 0 and 2π. The corresponding pair of (E, θ) are transformed to obtain the initial roll angle and angular velocity, which are then used as the initial conditions for the simulation of original system. It is also important to note that the estimates for higher initial energy levels result in more realizations that capsize and hence have more data points in the estimation of mean first passage times.

For the Monte Carlo simulations of the original system it is observed that approximately 53% of the simulations reach the capsize boundary before the maximum simulation time $T_{max} \approx 10(\mu_1)_{E_0=0}$. As the maximum simulation time is increased, the number of simulations reaching capsize increases. A choice of $T_{max} \approx 100(\mu_1)_{E_0=0}$ still results in 1% of the original system simulations not reaching capsize. Since not all simulations lead to capsize within a practically finite maximum simulation time, the data from simulations only allows for estimation of conditional first passage statistics conditioned on a finite exposure time ($T_{max} < \infty$).

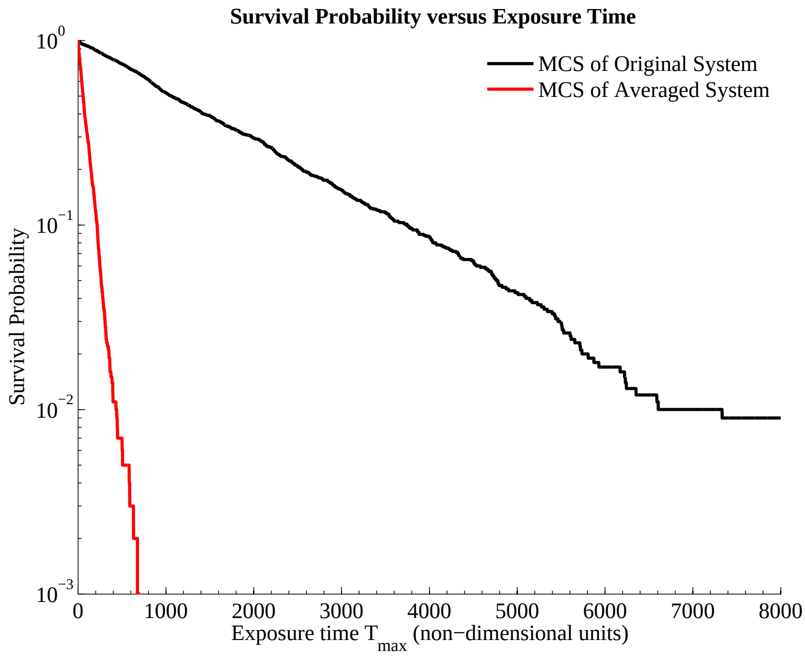

Figure 14: Survival probability (defined as the fraction of simulations which do not reach capsize in a specified exposure time) for $H_s = 8.0\ m$ and $T_p = 13.0\ sec$ and initial energy $E = 0.1764$

In order to estimate the unconditioned first passage statistics for the original system, the first passage behavior at larger exposure times is extrapolated based on the data from finite exposure time. A survival probability S is defined as the fraction of simulations that have not capsized in simulations within a specified exposure time T_{max}. Using data from 1000 simulations with $T_{max} \approx 100(\mu_1)_{E_0=0}$ for the case $H_s = 8.0\ m$ and $T_p = 13.0\ sec$, a plot of the survival probability versus the exposure time is generated and shown in Figure 14. Figure 14 reveals the exponential decrease of survival probability with exposure time for both the original and the averaged systems.

Due to the eventual softening nature of the nonlinear stiffness as seen in Figure 5, the process is not stationary after capsize occurs. However, up until the process reaches the capsize boundary, the process exhibits a stationary behavior. This is seen from the exponential decrease of the survival probability for both the averaged as well as the original system in Figure 14. The exponential decrease implies that the conditional up-crossing rate (conditioned on no up-crossing has occurred yet) is independent of the exposure time, which is only possible when a process is stationary.

It can be seen that the rate of decrease for the averaged system in Figure 14 is very rapid as compared to the original system. Hence, it is possible to choose a practical finite exposure time such that all simulations lead to capsize for the averaged system. For the original system this is not the case. In an ideal scenario with infinite exposure time ($T_{max} = \infty$) and infinite samples, the exponential decrease for the original system will extend indefinitely. Thus, we can assume

$$S = ce^{-\gamma T_{max}} \tag{91}$$

where $c \leq 1$ and γ are estimated by fitting an exponential function through the data with finite exposure time and finite samples. This means that as $T_{max} \to \infty$ the survival probability tends to zero and every simulation will eventually lead to capsize. However, as $T_{max} \to 0$ the survival probability approaches $c \leq 1$. This reflects the capsizes resulting from large transient dynamics. When starting at higher initial energy levels, a certain percentage of simulations capsize on account of transient dynamics and never reach steady state. This is evident in Figure 15 which shows the variation of survival probability of original system versus exposure time for various initial energy levels. As the initial energy level is lowered, $c \to 1$ and the transient response is not as significant and the system stops exhibiting almost instantaneous capsizes.

For convenience the subscript of T_{max} is dropped in the following analysis. Based on the assumption for survival probability, the cumulative probability of failure $F(T)$ is given by

$$F(T) = 1 - S = 1 - ce^{-\gamma T} \tag{92}$$

The probability density of failure $p_F(T)$ at all $T > 0$ is found by differentiating the cumulative probability of failure.

$$p_F(T) = \frac{dF}{dT} = \gamma c e^{-\gamma T} \tag{93}$$

However, it is important to note that there is a probability mass corresponding to $(1-c)$ at $T = 0$ which corresponds to almost instantaneous capsizes at higher initial energy levels. Assuming that the above is an acceptable approximation of the behavior for all time values then gives the mean first passage time as

$$\mu_1 = E[\tau_{FP}] = \int_0^\infty T p_F(T) dT + 0 \times (1-c) = \frac{c}{\gamma} \tag{94}$$

and the standard deviation of first passage time as

$$\sigma_{FP} = \sqrt{E[\tau_{FP}^2] - E[\tau_{FP}]^2} = \sqrt{\int_0^\infty \left(T - \frac{c}{\gamma}\right)^2 p_F(T) dT + \frac{c^2}{\gamma^2}(1-c)} = \frac{c}{\gamma}\sqrt{1 - c + c^2} \tag{95}$$

Figure 15 also shows the fitting of exponential function to the survival probability of the original system for simulation data with different initial energy levels. A comparison of the mean first passage estimates from Pontryagin equation, averaged system simulations, conditional estimates from original system simulations with finite exposure time and unconditional estimates from original system simulations using (94) and (95) are shown in Figure 16. A similar comparison for the standard deviation of the first passage time is shown in Figure 17.

It can be seen that the conditional estimates for the original system approach the unconditional estimates found using (94) and (95) as the exposure time is increased. However, the unconditioned first passage statistics from original system simulations are almost an order of magnitude higher than the calculations from Pontryagin equation and the estimates from averaged system simulations.

The difference between the first passage statistics from the original system simulations and the rest may be explained as follows. The stochastic averaging technique approximates the energy of the response as a Markov process. The approximated Markov process will, in general, be more irregular on a much smaller scale than the original process. When the bandwidth of the response displacement is large, the corresponding energy process will be quite irregular and the Markov approximation correctly accounts for this small scale irregularity. When the bandwidth of the response displacement is small as is for parametric response, the corresponding energy process is smoother. In such scenarios the Markov approximation is no longer accurate and results in irregularity in the approximated energy process that is not present in the original energy process. The effect of this irregularity is that the energy process for the averaged system is more likely to experience a high amplitude excursion as compared to the original system and thus results in lower mean first passage time.

This means that for a directly excited system, as the bandwidth of the excitation is increased the mean first passage time estimates from simulations of original system will approach the values found by solving the Pontryagin equations. Roberts [62] studied a directly excited Duffing oscillator with a softening spring and found that the mean first passage times from simulations asymptotically approach the values found by solving the Pontryagin equations as the bandwidth is increased. However, for the parametrically excited system due to the subharmonic resonance governing the dynamics, the displacement and velocity response spectra will always have a narrow bandwidth centered around the natural frequency of the unperturbed system ω_n. Thus, the results shown in Figure 16 and Figure 17 are expected, i.e. the estimates of mean

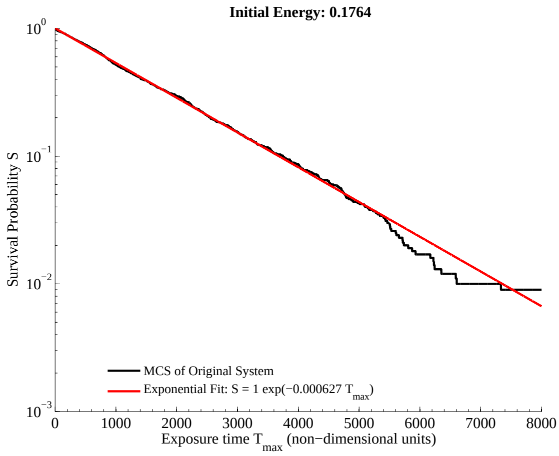

(a) $E = 0.1764$

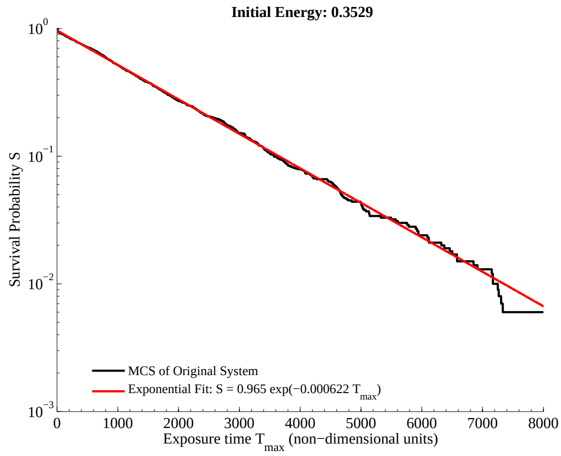

(b) $E = 0.3529$

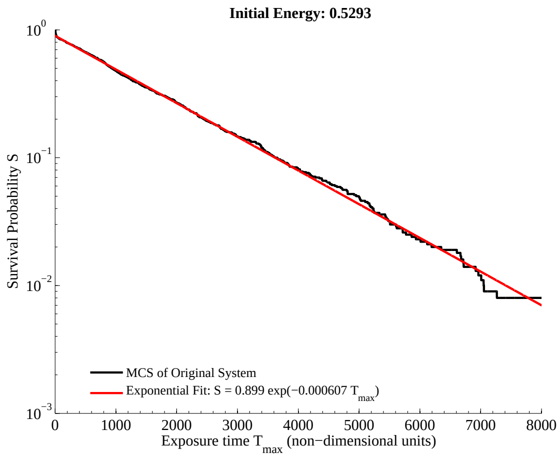

(c) $E = 0.5293$

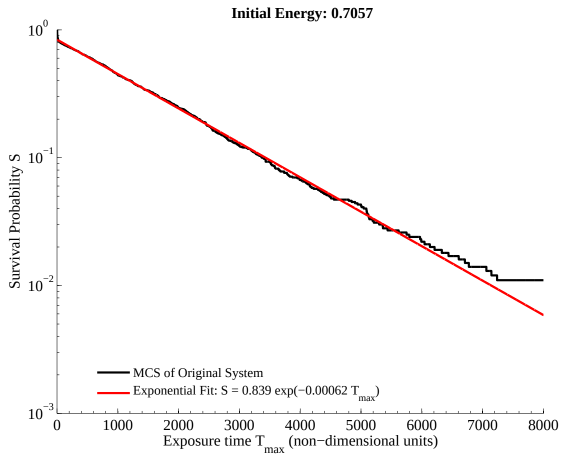

(d) $E = 0.7057$

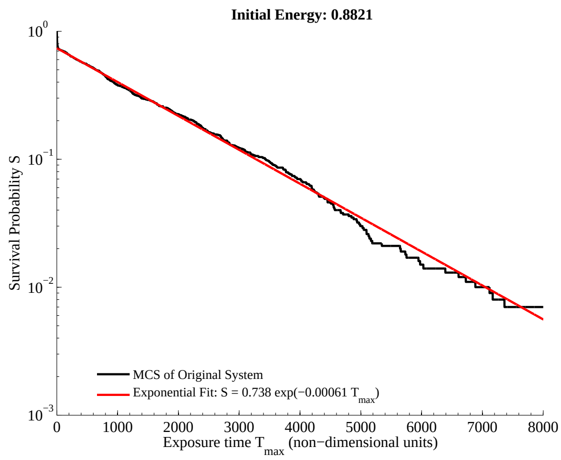

(e) $E = 0.8821$

Figure 15: Survival probability from Monte Carlo simulations of original system and its exponential fit for different initial energy levels for $H_s = 8.0\ m$ and $T_p = 13.0\ s$

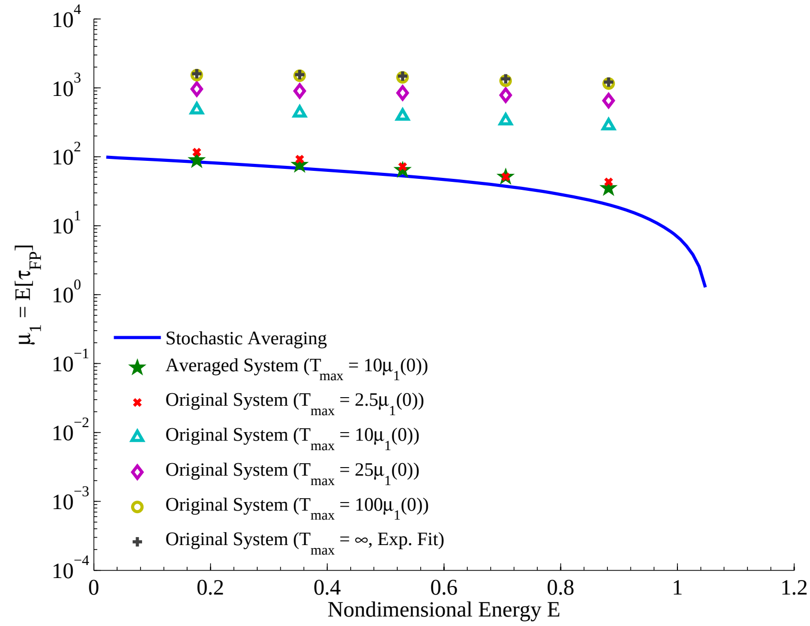

Figure 16: Comparison of mean first passage time calculated from stochastic averaging and Monte Carlo simulations of both original (conditional on finite exposure time T_{max}) and the averaged system for the case with $H_s = 8.0\ m$ and $T_p = 13.0\ sec$. The x-axis denotes the nondimensional initial energy of the system.

first passage times from stochastic averaging can be expected to be more conservative than observed mean first passage times from simulations of the original system. However, the conservative estimates still prove to be useful from a design perspective.

Ship design usually follows a iterative approach known as "design spiral" in naval architect terminology where the designer iterates through several interim designs before arriving at a final version which satisfies all the set requirements. Dynamic stability of a vessel typically requires time consuming simulations or expensive physical model tests and are therefore reserved only for the final design. Even today, dynamic stability is not always explicitly considered during the design process of a ship. However, the approach adopted in this paper allows for the design process to include dynamic stability explicitly. Since the computation time involved in solving the Pontryagin equations is minuscule, the mean first passage times provide an effective design assessment criterion that can efficiently be used to compare the relative stability of various designs.

8. Conclusion

In this paper a new approach to effectively estimate the vulnerability of a vessel to parametric roll in irregular seas is developed. A previously developed analytical model (Volterra $\overline{GZ}$ method) for parametric roll of ship in random seaway is analyzed using the stochastic averaging approach. The energy in the roll mode of motion is shown to be slowly varying compared to excitation time scale and is hence approximated as a Markov process. A simple analytical criterion in terms of character value c_0 of a stochastically averaged system is found that allows a designer to quickly check if a sea state is critical ($c_0 > 1$) for experiencing parametric roll motion. If the vessel satisfies the vulnerability check, the stability of the design is then calculated in terms of the mean first passage time taken by the system to capsize. The mean first passage times of energy to reach the capsizing boundary are calculated by solving the Pontryagin equation numerically and are shown to be in good agreement with Monte Carlo simulations of the averaged system. It is found that the mean first passage times from use of the Pontryagin equation are sometimes significantly more conservative than those from Monte Carlo simulations of the original equations. This, though, assures that use of the Pontryagin equation gives safe results for boundaries of failure.

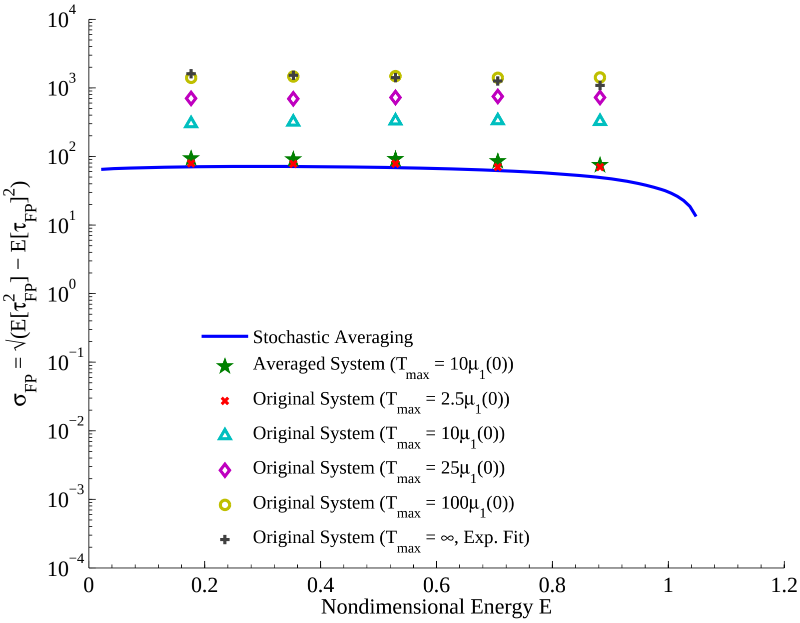

Figure 17: Comparison of standard deviation of first passage time calculated from stochastic averaging and Monte Carlo simulations of both original (conditional on finite exposure time T_{max}) and the averaged system for the case with $H_s = 8.0\ m$ and $T_p = 13.0\ sec$. The x-axis denotes the nondimensional initial energy of the system.

The mean first passage time of the roll system computed by this approach is extremely quick due to its semi-analytic nature and provides an effective estimate of stability of the ship when subjected to parametric excitation without the need to simulate long time histories. Since the involved computation is minuscule, it is an ideal tool for a ship designer to evaluate and compare the vulnerability of various interim hull form designs iterated through the design spiral. This approach, while having a strong theoretical foundation, is also in line with the second generation level 2 criterion being discussed by International Maritime Organization (IMO).

References

[1] France W, Levadou M, Treakle TW, Paulling JR, Michel RK, Moore C. An investigation of head-sea parametric rolling and its influence on container lashing systems. Marine Technology 2003; 40(1):1–19.

[2] Carmel S. Study of Parametric Rolling Event on a Panamax Container Vessel. Transportation Research Record: Journal of the Transportation Research Board 2006; 1963:56–63.

[3] Umeda N, Francescutto A. Current state of the second generation intact stability criteria achievements and remaining issues. In: Proceedings of the 15th International Ship Stability Workshop. June; Stockholm, Sweden; 2016, p. 13–5.

[4] Somayajula AS. Reliability Assessment of Hull Forms Susceptible to Parametric Roll in Irregular Seas. Phd dissertation; Texas A&M University; College Station, TX; 2017.

[5] Somayajula A, Falzarano J. Volterra GZ approach a new method to accurately calculate the non-linear and time-varying roll restoring arm of ships in irregular longitudinal seas. Ships and Offshore Structures 2018; 13(4):423–31.

[6] Somayajula A, Falzarano J. Large-amplitude time-domain simulation tool for marine and offshore motion prediction. Marine Systems & Ocean Technology 2015; 10(1):1–17.

[7] Chai W, Naess A, Leira BJ, Carlo M. Stochastic dynamic analysis and reliability of a vessel rolling in random beam seas. Journal of Ship Research 2015; 59(2):113–31.

[8] Roberts JB, Spanos PD. Random Vibration and Statistical Linearization. Mineola: Dover Publications; 2003.

[9] Caughey T. On the response of non-linear oscillators to stochastic excitation. Probabilistic Engineering Mechanics 1986; 1(1):2–4.

[10] Lutes LD. Approximate technique for treating random vibration of hysteretic systems. Journal of the Acoustical Society of America 1970; 48(1B):299–306.

[11] Stratonovich RL. Topics in the Theory of Random Noise: Volume I. New York: Gordon and Breach, Science Publishers, Inc.; 1963.

[12] Stratonovich RL. Topics in the Theory of Random Noise: Volume II. New York: Gordon and Breach, Science Publishers, Inc.; 1967.
[13] Su Z, Falzarano JM. Gaussian and non-Gaussian cumulant neglect application to large amplitude rolling in random waves. International Shipbuilding Progress 2011; 58:97–113.
[14] Spanos PT. Stochastic analysis of oscillators with non-linear damping. International Journal of Non-Linear Mechanics 1978; 13(4):249–60.
[15] Roberts J. A stochastic theory for nonlinear ship rolling in irregular seas. Journal of Ship Research 1982; 26(4):229–45.
[16] Lutes LD, Sarkani S. Random Vibrations: Analysis of Structural and Mechanical Systems. 1st ed.; Boston: Elsevier Butterworth-Heinemann; 2004. ISBN 978-0-7506-7765-3.
[17] Chai W, Naess A, Leira BJ. Filter models for prediction of stochastic ship roll response. Probabilistic Engineering Mechanics 2015; 41:104–14.
[18] Caughey T. Nonlinear theory of random vibrations. In: Yih CS, editor. Advances in Applied Mechanics (Volume 11). New York: Academic Press; 1971, p. 209–53.
[19] Mayfield W. A sequence solution to the Fokker-Planck equation. IEEE Transactions on Information Theory 1973; 19(2):165–76.
[20] Wehner MF, Wolfer WG. Numerical evaluation of path-integral solutions to Fokker-Planck equations. Physical Review A 1983; 27(5):2663–70.
[21] Jamnongpipatkul A. Ship rolling motion subjected to colored noise excitation. Masters thesis; Texas A&M University; College Station; 2010.
[22] Li J, Chen J. Stochastic Dynamics of Structures. Chichester, UK: John Wiley & Sons, Ltd; 2009. ISBN 9780470824269.
[23] Naess A, Moe V. Efficient path integration methods for nonlinear dynamic systems. Probabilistic Engineering Mechanics 2000; 15(2):221–31.
[24] Iourtchenko D, Mo E, Naess A. Reliability of Strongly Nonlinear Single Degree of Freedom Dynamic Systems by the Path Integration Method. Journal of Applied Mechanics 2008; 75(6):061016.
[25] Di Matteo A, Kougioumtzoglou IA, Pirrotta A, Spanos PD, Di Paola M. Stochastic response determination of nonlinear oscillators with fractional derivatives elements via the Wiener path integral. Probabilistic Engineering Mechanics 2015; 38:127–35.
[26] Psaros AF, Kougioumtzoglou IA, Petromichelakis I. Sparse representations and compressive sampling for enhancing the computational efficiency of the Wiener path integral technique. Mechanical Systems and Signal Processing 2018; 111:87–101.
[27] Francescutto A, Naito S. Large amplitude rolling in a realistic sea. International shipbuilding progress 2004; 51(2):221–35.
[28] Su Z, Falzarano JM. Gaussian and Non Gaussian Response of Ship Rolling in Random Beam Waves. In: Proceedings of the12th International Ship Stability Workshop. Washington DC, USA; 2011, p. 189–93.
[29] Papanicolaou GC, Kohler W. Asymptotic theory of mixing stochastic ordinary differential equations. Communications on Pure and Applied Mathematics 1974; 27(5):641–68.
[30] Khas'minskii R. A limit theorem for the solutions of differential equations with random right-hand sides. Theory of Probability & Its Applications 1966; 11(3):390–406.
[31] Roberts J. Averaging methods in random vibration. Tech. Rep.; Technical University Denmark; Lyngby, Denmark; 1989.
[32] Lin Y, Cai G. Probabilistic Structural Dynamics: Advanced Theory and Applications. 1st ed.; New York: McGraw-Hill; 2004. ISBN 0071438009.
[33] Bogoliubov NN, Mitropolski YA. Asymptotic Methods in the Theory of Non-linear Oscillations. 1st ed.; New York: Gordon and Breach; 1961.
[34] Zhu WQ. Stochastic averaging methods in random vibration. Applied Mechanics Reviews 1988; 41(5):189.
[35] Chai W, Dostal L, Naess A, Leira BJ. A comparative study of the stochastic averaging method and the path integration method for nonlinear ship roll motion in random beam seas. Journal of Marine Science and Technology 2018; 23(4):854–65.
[36] Su Z, Falzarano JM. Markov and Melnikov based methods for vessel capsizing criteria. Ocean Engineering 2013; 64:146–52.
[37] Su Z. Nonlinear response and stability analysis of vessel rolling motion in random waves using stochastic dynamical systems. Phd dissertation; Texas A&M University; College Station; 2012.
[38] Roberts J. The Effect of Parametric Excitation on Ship Rolling Motion in Random Waves. Journal of Ship Research 1982; 26(4):246–53.
[39] Bulian G. Development of analytical nonlinear models for parametric roll and hydrostatic restoring variations in regular and irregular waves. Phd dissertation; Università degli studi di Trieste; Trieste; 2006.
[40] Francescutto A, Bulian G, Lugni C. Nonlinear and stochastic aspects of parametric rolling modeling. Marine Technology 2004; 41(2):74–81.
[41] Dostal L, Kreuzer E, Sri Namachchivaya N. Non-standard stochastic averaging of large-amplitude ship rolling in random seas. Proceedings of the Royal Society A: Mathematical, Physical and Engineering Sciences 2012; 468(April):4146–73.
[42] Dostal L. Assessment of Extreme Rolling of Ships in Random Seas. In: Proceedings of the ASME 2014 33rd International Conference on Ocean, Offshore and Arctic Engineering. 2014,.
[43] Somayajula A, Falzarano J. Parametric Roll Vulnerability of Ships using Markov and Melnikov approaches. Nonlinear Dynamics (Under Review) 2019;.
[44] Neves MA, Rodriguez C. A coupled third order model of roll parametric resonance. In: Soares CG, Garbatov Y, Fonseca N, editors. Maritime Transportation and Exploitation of Ocean and Coastal Resources - Volume 1: Vessels for Maritime Transportation. London, UK: Taylor and Francis Group Plc; 2005, p. 243–53.
[45] Umeda N, Hashimoto H, Vassalos D. Nonlinear dynamics on parametric roll resonance with realistic numerical modelling. International Shipbuilding Progress 2004; 51(2):205–20.

[46] Bulian G, Francescutto A. On the effect of stochastic variations of restoring moment in long-crested irregular longitudinal sea. International Shipbuilding Progress 2007; 54(4):227–48.
[47] Moideen H, Somayajula A, Falzarano JM. Application of Volterra series analysis for parametric rolling in irregular seas. Journal of Ship Research 2014; 58(2):97–105.
[48] Somayajula AS, Falzarano JM. Validation of Volterra series approach for modelling parametric rolling of ships. In: Proceedings of 34th International Conference on Ocean, Offshore and Arctic Engineering - Volume 11: Prof. Robert F. Beck Honoring Symposium on Marine Hydrodynamics. St. John's, NL, Canada: ASME. ISBN 978-0-7918-5659-8; 2015, p. V011T12A043.
[49] Somayajula AS, Falzarano JM. Non-linear dynamics of parametric roll of container ship in irregular seas. In: Proceedings of 33rd International Conference on Ocean, Offshore and Arctic Engineering - Volume 7: Ocean Space Utilization; Professor Emeritus J. Randolph Paulling Honoring Symposium on Ocean Technology. San Francisco: ASME. ISBN 978-0-7918-4549-3; 2014, p. V007T12A018.
[50] Somayajula A, Guha A, Falzarano J, Chun HH, Jung KH. Added resistance and parametric roll prediction as a design criteria for energy efficient ships. Ocean Systems Engineering 2014; 4(2):117–36.
[51] Somayajula AS, Falzarano J. A comparative assessment of simplified models for simulating parametric roll. Journal of Offshore Mechanics and Arctic Engineering 2017; 139(2):021103.
[52] Somayajula A, Falzarano J. Estimation of roll motion parameters using R-MISO system identification technique. In: Chung JS, Muskulus M, Kokkinis T, Wang AM, editors. 26th International Offshore and Polar Engineering (ISOPE 2016) Conference; vol. 3. Rhodes (Rodos), Greece: International Society of Offshore and Polar Engineers (ISOPE); 2016, p. 568–74.
[53] Somayajula A, Falzarano J. Critical assessment of reverse-MISO techniques for system identification of coupled roll motion of ships. Journal of Marine Science and Technology 2017; 22(2):231–44.
[54] Somayajula A, Falzarano J. Application of advanced system identification technique to extract roll damping from model tests in order to accurately predict roll motions. Applied Ocean Research 2017; 67:125–35.
[55] Himeno Y. Ship Roll Damping- Jure and Marine Engineering the University of Michigan. Tech. Rep. 239; University of Michigan; Ann Arbor, MI, USA; 1981.
[56] Ikeda Y, Himeno Y, Tanka N. A Prediction Method for Ship Roll Damping. Tech. Rep.; University of Osaka Prefecture; Osaka, Japan; 1978.
[57] Falzarano J, Somayajula A, Seah R. An overview of the prediction methods for roll damping of ships. Ocean Systems Engineering 2015; 5(2):55–76.
[58] Roberts JB, Vasta M. Energy-based stochastic estimation for nonlinear oscillators with random excitation. Journal of Applied Mechanics 2000; 67(4):763–71.
[59] Feller W. Diffusion processes in one dimension. Transactions of the American Mathematical Society 1954; 77(1):1–31.
[60] Cai GQ, Lin YK. On statistics of first-passage failure. Journal of Applied Mechanics 1994; 61(1):93.
[61] Higham. DJ. An algorithmic introduction to numerical simulation of stochastic differential equations. SIAM Review 2001; 43(3):525–46.
[62] Roberts J. Response of an oscillator with non-linear damping and a softening spring to non-white random excitation. Probabilistic engineering mechanics 1986; 1(1):40–8.

Appendix A. Derivation of the Singular Boundary Condition of Pontryagin Equation at $E = 0$

Since we are interested in the boundary condition at $E = 0$, the nonlinear oscillator can be linearized in the vicinity of the boundary. Thus considering only the linear stiffness and linear damping to be dominant near $E = 0$, the original oscillator given by (11) can be approximated as

$$\ddot{x} + \varepsilon^2 \delta_1 \dot{x} + x + \varepsilon p_1(t) x = 0 \tag{A.1}$$

The energy and phase in this case are defined as

$$E = \frac{\dot{x}^2}{2} + \frac{x^2}{2} \tag{A.2}$$

$$\theta = \tan^{-1}\left(\frac{-\dot{x}}{x}\right) \tag{A.3}$$

The displacement x and velocity $\dot{x}$ in the linear case are given by

$$x = \sqrt{2E}\cos(\theta) \tag{A.4}$$

$$\dot{x} = -\sqrt{2E}\sin(\theta) \tag{A.5}$$

The differential equation governing $E(t)$ and $\theta(t)$ are obtained by differentiating (A.2) and (A.3) with respect to time t respectively.

$$\dot{E} = \varepsilon^2 \left(-2E\delta_1 \sin^2(\theta)\right) + \varepsilon p_1(t) E \sin(2\theta) \tag{A.6}$$

$$\dot{\theta} = 1 + \varepsilon^2 \left(-\frac{\delta_1}{2}\sin(2\theta)\right) + \varepsilon p_1(t)\cos^2(\theta) \tag{A.7}$$

Defining a new phase process $\lambda(t) = \theta(t) - t$,

$$\dot{E} = \varepsilon^2 \left(-2E\delta_1 \sin^2(\theta)\right) + \varepsilon p_1(t) E \sin(2\theta) \tag{A.8}$$

$$\dot{\lambda} = \varepsilon^2 \left(-\frac{\delta_1}{2}\sin(2\theta)\right) + \varepsilon p_1(t)\cos^2(\theta) \tag{A.9}$$

Thus the vector process $\boldsymbol{Z}(t) = \begin{Bmatrix} E(t) \\ \lambda(t) \end{Bmatrix}$ is a slowly varying with time and is given by

$$\dot{\boldsymbol{Z}}(t) = \begin{bmatrix} \dot{E} \\ \dot{\lambda} \end{bmatrix} = \varepsilon^2 \boldsymbol{a}(\boldsymbol{Z}) + \varepsilon \boldsymbol{b}(t, \boldsymbol{Z}) \tag{A.10}$$

where

$$\boldsymbol{a}(\boldsymbol{Z}) = \begin{bmatrix} a_1(E,\theta) \\ a_2(E,\theta) \end{bmatrix} = \begin{bmatrix} -2E\delta_1 \sin^2(\theta) \\ -\frac{\delta_1}{2}\sin(2\theta) \end{bmatrix} \tag{A.11}$$

$$\boldsymbol{b}(t, \boldsymbol{Z}) = \begin{bmatrix} b_1(t,E,\theta) \\ b_2(t,E,\theta) \end{bmatrix} = \begin{bmatrix} p_1(t) E \sin(2\theta) \\ p_1(t)\cos^2(\theta) \end{bmatrix} \tag{A.12}$$

Applying the technique of stochastic averaging as described in section 4, the drift and diffusion coefficients of the linear system are given by

$$\boldsymbol{m} = \boldsymbol{A}(E) + \int_{-\infty}^{0} \left\langle E\left[\left(\frac{\partial \boldsymbol{b}}{\partial \boldsymbol{Z}}\right)_t (\boldsymbol{b})_{t+\tau}\right]\right\rangle d\tau \tag{A.13}$$

$$\boldsymbol{D} = \boldsymbol{\sigma}\boldsymbol{\sigma}^T = \int_{-\infty}^{\infty} \left\langle E\left[(\boldsymbol{b})_t \, (\boldsymbol{b})_{t+\tau}^T\right]\right\rangle d\tau \tag{A.14}$$

where

$$\frac{\partial \boldsymbol{b}}{\partial \boldsymbol{Z}} = \begin{bmatrix} \frac{\partial b_1}{\partial E} & \frac{\partial b_1}{\partial \lambda} \\ \frac{\partial b_2}{\partial E} & \frac{\partial b_2}{\partial \lambda} \end{bmatrix} \tag{A.15}$$

$$\boldsymbol{A}(E) = \begin{bmatrix} A_1(E) \\ A_2(E) \end{bmatrix} = \langle \boldsymbol{a}(E,\theta_0) \rangle = \frac{1}{T(E)} \int_0^{T(E)} \boldsymbol{a}(E,\theta_0) dt \tag{A.16}$$

Note that $\langle [.] \rangle$ denotes the time average over the unperturbed system period $T(E)$ and is given by

$$\langle [\ .\ ] \rangle = \frac{1}{T(E)} \int_0^{T(E)} [\ .\ ] dt \tag{A.17}$$

where the unperturbed system period $T(E)$ is given by

$$T(E) = \oint \left|\frac{dx}{\dot{x}}\right| = 4\int_0^b \frac{dx}{\sqrt{2E}\sin(\theta)} = 4\int_{-\frac{\pi}{2}}^{0} \frac{\sqrt{2E}\sin(\theta)d\theta}{\sqrt{2E}\sin(\theta)} = 2\pi \tag{A.18}$$

$$A_1(E) = \frac{1}{2\pi}\int_0^{T(E)} -\delta_1 2E\sin^2(\theta_0)dt = \frac{1}{2\pi}\int_0^{2\pi} -\delta_1 2E\sin^2(t)dt = -\delta_1 E \tag{A.19}$$

$$A_2(E) = \frac{1}{2\pi}\int_0^{T(E)} -\frac{\delta_1}{2}\sin(2\theta_0)dt = \frac{1}{2\pi}\int_0^{2\pi} -\frac{\delta_1}{2}\sin(2t)dt = 0 \tag{A.20}$$

The drift and diffusion coefficients corresponding to the energy process are given by

$$\begin{aligned} m_1 &= A_1(E) + \int_{-\infty}^{0} \left\langle E\left[\left(\frac{\partial b_1}{\partial E}\right)_t (b_1)_{t+\tau} + \left(\frac{\partial b_1}{\partial \lambda}\right)_t (b_2)_{t+\tau}\right]\right\rangle d\tau \\ &= \left(\pi S_{11}^{(c)}(2) - \delta_1\right) E \end{aligned} \tag{A.21}$$

$$D_{11} = \int_{-\infty}^{\infty} \left\langle E\left[(b_1)_t\,(b_1)_{t+\tau}^T\right]\right\rangle d\tau = \pi S_{11}^{(c)}(2)E^2 \tag{A.22}$$

$$D_{12} = \int_{-\infty}^{\infty} \left\langle E\left[(b_1)_t\,(b_2)_{t+\tau}^T\right]\right\rangle d\tau = 0 \tag{A.23}$$

Note that since $D_{12} = 0$, the energy process is also a Markov process itself in the vicinity of $E = 0$. It can be seen from (A.21) that the drift exponent is $\alpha_0 = 2$. Similarly from (A.22) it can be seen that diffusion exponent $\beta_0 = 1$. The character value c_0 is given by

$$c_0 = \frac{2m_1(E)(E-0)^{\alpha_0-\beta_0}}{\sigma_{11}^2(E)} = 2\left(1 - \frac{\delta_1}{\pi S_{11}^{(c)}(2)}\right) \tag{A.24}$$

According to Lin and Cai [32], a drift exponent $\beta_0 = 1$ and a diffusion exponent $\alpha_0 = 2$ corresponds to a natural boundary at $E = 0$. The character value c_0 decides if the boundary is further strictly ($c_0 = 1$), attractively ($c_0 < 1$) or repulsively natural ($c_0 > 1$).

As described in section 6, the Pontryagin formulation assumes that every sample path will eventually reach the critical boundary $E = E_c$ (given by $\mu_1(E_c, E_0)|_{E_0=0} < \infty$). Thus only those boundary conditions which allow for this possibility are admissible. In case of a strictly natural or attractively natural boundary, not every sample path starting at or near $E = 0$ will necessarily reach the critical boundary $E = E_c$ [32, 60]. Thus the Pontryagin equation is applicable only if the boundary is a repulsively natural boundary given by $c_0 > 1$. In this case, the Pontryagin equation is given by

$$\frac{\pi S_{11}^{(c)}(2)}{2}E^2\frac{d^2\mu_1}{dE^2} + (\pi S_{11}^{(c)}(2) - \delta_1)E\frac{d\mu_1}{dE} + 1 = 0 \tag{A.25}$$

Since the above equation is an Euler type differential equation, it can be integrated to yield

$$E\frac{d\mu_1}{dE}(E) = C_1 E^{\left[\frac{2\delta_1}{\pi S_{11}^{(c)}(2)} - 2\right]} - \frac{2}{\left(\pi S_{11}^{(c)}(2) - 2\delta_1\right)} \tag{A.26}$$

Imposing the boundary condition of the form (86) gives $C_1 = 0$ and results in the boundary condition given by (89). Applying a similar technique to Pontryagin equation for mean squared first passage time μ_2 results in the boundary condition given by (90).